UV-Indien network: ground-based measurements dedicated to the monitoring of UV radiation over the western Indian Ocean

Kevin Lamy, Thierry Portafaix, Colette Brogniez, Kaisa Lakkala, Mikko R A Pitkänen, Antti Arola, Jean-Baptiste Forestier, Vincent Amelie, Mohamed Abdoulwahab Toihir, Solofoarisoa Rakotoniaina

Earth Syst. Sci. Data, 13, 4275–4301, 2021
https://doi.org/10.5194/essd-13-4275-2021

Open Access Earth System Science Data

UV-Indien network: ground-based measurements dedicated to the monitoring of UV radiation over the western Indian Ocean

Kevin Lamy[1], Thierry Portafaix[1], Colette Brogniez[2], Kaisa Lakkala[3,4], Mikko R. A. Pitkänen[4], Antti Arola[4], Jean-Baptiste Forestier[1], Vincent Amelie[5], Mohamed Abdoulwahab Toihir[6], and Solofoarisoa Rakotoniaina[7]

[1]LACy, Laboratoire de l'Atmosphère et des Cyclones (UMR 8105 CNRS, Université de La Réunion, Météo-France), Saint-Denis de La Réunion, France
[2]LOA, Laboratoire d'Optique Atmosphérique (Univ. Lille, CNRS – UMR 8518) Lille, France
[3]Space and Earth Observation Centre, Finnish Meteorological Institute, Sodankylä, Finland
[4]Climate Research Programme, Finnish Meteorological Institute, Kuopio, Finland
[5]Seychelles Meteorological Authority, Mahé, Seychelles
[6]Agence Nationale de l'Aviation Civile et de la Météorologie, Moroni, Comoros
[7]IOGA, Institute and Observatory of Geophysics of Antananarivo (IOGA), University of Antananarivo, Antananarivo, Madagascar

Correspondence: Kevin Lamy (kevin.lamy@univ-reunion.fr)

Received: 22 February 2021 – Discussion started: 3 March 2021
Revised: 10 July 2021 – Accepted: 16 July 2021 – Published: 2 September 2021

Abstract. Within the framework of the UV-Indien network, nine ground stations have been equipped with ultraviolet broadband radiometers, five of them have also been equipped with an all-sky camera, and the main station in Saint-Denis de la Réunion is also equipped with a spectroradiometer. These stations are spatially distributed to cover a wide range of latitudes, longitudes, altitudes, and environmental conditions in five countries of the western Indian Ocean region (Comoros, France, Madagascar, Mauritius, and Seychelles), a part of the world where almost no measurements have been made so far. The distribution of the stations is based on the scientific interest of studying ultraviolet radiation not only in relation to atmospheric processes but also in order to provide data relevant to fields such as biology, health (prevention of skin cancer), and agriculture. The main scientific objectives of this network are to study the annual and inter-annual variability in the ultraviolet (UV) radiation in this area, to validate the output of numerical models and satellite estimates of ground-based UV measurements, and to monitor UV radiation in the context of climate change and projected ozone depletion in this region. A calibration procedure including three types of calibrations responding to the various constraints of sustaining the network has been put in place, and a data processing chain has been set up to control the quality and the format of the files sent to the various data centres. A method of clear-sky filtering of the data is also applied. Here, we present an intercomparison with other datasets, as well as several daily or monthly representations of the UV index (UVI) and cloud fraction data, to discuss the quality of the data and their range of values for the older stations (Antananarivo, Anse Quitor, Mahé, and Saint-Denis). Ground-based measurements of the UVI are used to validate satellite estimates – Ozone Monitoring Instrument (OMI), the TROPOspheric Monitoring Instrument (TROPOMI), and the Global Ozone Monitoring Experiment (GOME) – and model forecasts of UVI – Tropospheric Emission Monitoring Internet Service (TEMIS) and Copernicus Atmospheric Monitoring Service (CAMS). The median relative differences between satellite or model estimates and ground-based measurements of clear-sky UVI range between −34.5 % and 15.8 %. Under clear skies, the smallest UVI median difference between the satellite or model estimates and the measurements made by ground-based instruments is found to be 0.02 (TROPOMI), 0.04 (OMI), −0.1 (CAMS), and −0.4 (CAMS) at Saint-Denis, Antananarivo,

Anse Quitor, and Mahé, respectively. The diurnal variability in UVI and cloud fraction, as well as the monthly variability in UVI, is evaluated to ensure the quality of the dataset. The data used in this study are available at https://doi.org/10.5281/zenodo.4811488 (Lamy and Portafaix, 2021a).

1 Introduction

The sun produces a broad spectrum of radiation, in which wavelengths between 100 and 400 nm correspond to ultraviolet radiation (UVR). The UVR that reaches the Earth's surface has a direct effect on human health, terrestrial and aquatic ecosystems, and the degradation of materials (Bernhard et al., 2020).

UV has important effects on human health. These effects can be beneficial or harmful. For example, human exposure to UV-B ensures the synthesis of vitamin D, which is essential for bone mineralisation. UVR is also known to be a powerful virus killer, which can explain some epidemiological pattern (Duan et al., 2003). On the other hand, UV-B can have a harmful effect by altering the DNA of cells. For humans, an increase in UV-B radiation increases the risk of skin cancer and the occurrence of cataracts and weakens the immune system.

The UV Index (UVI) was defined by the World Health Organization (WHO, 1995) to measure the amount of sunburn-producing UV radiation that reaches the surface. If the UVI is above 3, protection is necessary, and, above 8, prolonged exposure can become dangerous. Indices above 11 are considered extreme.

Naturally, the geographical area corresponding to the tropics of the southern hemisphere (tropical and ocean-dominated environment) exposes populations to high levels of UV radiation. This is because the zenith angles of the sun close to noon are very small all year round, and the amounts of stratospheric ozone or atmospheric aerosols are lower than at higher latitudes in continental regions. This is the case in most of the southern Indian Ocean (La Réunion, Madagascar, Mauritius, Seychelles, Comoros). UV indices in these regions can exceed 10 almost all year round, which implies serious consequences for the health of the populations. For example, dermatologists in Reunion Island (21° S, 55.5° E) have noted a rapid increase in sun-induced skin lesions (Observatoire Régional de la Santé de La Réunion, 2008). The number of these lesions is currently tripling every 10 years, with an accelerating progression, and more than 2 % of the population is affected. Radiation doses received by particularly exposed populations (children and outdoor workers) exceed dangerous thresholds in this region of the Indian Ocean almost all year round (Wright et al., 2013). Finally, it can be noted that all skin phototypes are concerned, including phototypes 5 and 6 (Sitek et al., 2016). An important part of this observed increase can be explained by lifestyle changes, with an expansion of seaside activities and a constant increase in exposure to the sun. The development of tourism, especially local tourism, is a determining factor.

When UV radiation penetrates the atmosphere, its intensity along the atmospheric path and on the ground depends on various parameters, including geometric or geographical factors such as the solar zenith angle (SZA), latitude, and altitude. Cloud cover plays an important role, generally reducing the intensity of radiation, although under certain conditions cloud cover can also increase the intensity, as is the case of fractional cloud cover (Sabburg and Wong, 2000). Aerosols, small particles of natural (marine aerosols, volcanic) or anthropogenic (biomass fires, fossil fuel combustion) origin, scatter and absorb UV radiation. If present in large quantities, they can strongly affect surface UV radiation or radiative forcing. The reflectivity of a surface, or albedo, is also involved in modulating the intensity of radiation, and, finally, the concentrations of certain gases, such as ozone, in the atmosphere play an essential role. The amount of ozone (O_3) in the stratosphere largely drives UV levels on the ground because ozone has a high absorption capacity in the UV wavelengths. O_3 is produced in the tropics under the influence of strong solar radiation and is transported towards the poles by the Brewer–Dobson circulation (BDC).

Ozone concentrations have been significantly depleted over the past 35 years due to emissions of halocarbons, which are both powerful greenhouse gases (GHGs) and ozone-depleting substances (ODSs). The Montreal Protocol (1987) and its amendments are an undisputed success in environmental policy making and have slowly brought ODS amounts down almost to historical levels (Chipperfield et al., 2015).

However, for the evolution of stratospheric ozone beyond the middle of the 21st century, ODS emissions will be minimal and their atmospheric concentrations will continue to decrease and be largely determined by the concentrations of certain GHGs such as CO_2, N_2O, and CH_4 (Eyring et al., 2013). On the other hand, the increase in CO_2 is expected to accelerate the BDC (Butchart, 2014; WMO, 2018). Ozone will then be transported more rapidly from the tropics to the poles, and thus the total ozone column (TOC) will increase in mid-latitudes and decrease in the tropics. Since UV radiation at the surface is directly dependent on the total ozone column, UV can be expected to decrease in mid-latitudes and increase in the tropics (Butler et al., 2016; Lamy et al., 2019). Therefore, climate change, linked to the accumulation of greenhouse gases in the atmosphere, is also one of the phenomena identified to explain the increasing levels of exposure to UV radiation in the tropics.

The western Indian Ocean is mainly located in the tropical region of the southern hemisphere. This part of the world is therefore potentially impacted by the changes in radiation described above. However, this geographical area suffers from a very large measurement deficit, both for ozone and UV radiation on the ground. Studies associated with these topics are sparse in the literature. The originality of Reunion Island is that it is located in the heart of this region and has benefited from high-quality measurements of ozone and aerosols for several decades thanks to OPAR (Reunion's Atmospheric Physics Observatory). Within the framework of various programmes funded by Europe, Reunion Council or CNES (French Space Agency), the University of Reunion Island has developed a specialised network for the measurement of UV radiation and cloud cover in the south-western part of the Indian Ocean, known as the UV-Indien network. The datasets presented here are original and, as mentioned, concern an extremely poorly measured region of the globe, which highlights their importance. They include the UV index at nine stations and the cloud fraction (CF) measured at four stations. These measurements are ideally suited for assessing the effect of UV radiation on the health of people or ecosystems in this region.

2 UV-Indien network

2.1 Scientific objectives

The UV-Indien measurement network proposes to answer the following scientific questions:

- What is the annual and inter-annual variability in UV radiation at the scale of the western Indian Ocean area?
- How is UV radiation impacted by regular episodes of ozone-rich or ozone-poor air mass filaments over different places?
- Are chemistry transport models or regional climate models, coupled with radiative transfer models (RTMs), reliable for predicting the evolution of UV radiation in the southern tropics?
- How will UVR evolve by the end of this century in the Indian Ocean, in the context of climate change and the predicted 3 %–4 % decrease in ozone?

2.2 Selection and characterisation of sites

Although the selection of the instrumented sites of the UV-Indien network was conditioned by financial, technical, and logistical feasibility constraints, the choice of the sites where the stations were implanted was also based on several scientific criteria: a spatial distribution of stations that is as homogeneous as possible over a region where the majority of the land area is located in the western part (an essential criterion for obtaining the highest geographical representativeness in order to be able to validate the outputs of climate models for UV forecasting in the region); a diversity of environmental conditions (between urban and rural sites, different degrees of pollution, close to the coast or not, at low or high altitude); the presence of scientific partners on site; and the interest of UV measurements for other scientific disciplines. For example, the site of Anse Quitor, Rodrigues, is situated on the roof of the François Legat turtle reserve. This reserve aims to preserve giant tortoises and monitor their behaviour and biology, so it is of interest to use environmental data such as UV radiation and cloudiness. The sites of the UV-Indien network are presented in Table 1 and are indicated on the map (Fig. 1).

The site of Saint-Denis, Reunion, is the main site of the UV-Indien network. UV measurements have been carried out since January 2009 with the Bentham DTMc300 spectroradiometer (affiliated with the Network for the Detection of Atmospheric Composition Change – NDACC) and since December 2016 with the Kipp and Zonen UVS-E-T radiometer. Cloudiness measurements have been carried out since October 2016. This site has the advantage of being co-located with several other instruments, allowing detailed studies of physical processes. These include the UV–visible spectrometer SAOZ (Système D'Analyse par Observations Zénithales) (Pastel et al., 2014; Toihir et al., 2018), which measures the total column of ozone and nitrogen dioxide and is part of the NDACC network, or the sun photometer CIMEL (Kabanov et al., 2001), which carries out measurements of the optical and microphysical properties of aerosols and is part of AERONET (AErosol RObotic NETwork; Holben et al., 1998). The environment of Saint-Denis is urban and slightly polluted by heavy road traffic despite the regular advection of air by the trade winds. This site is located on the coast at an altitude of 82 m a.s.l. and is surrounded by high reliefs of 500 to 1500 m altitude. The climate is tropical and marked by two distinct seasons: a rainy season in the southern summer and a dry season in the southern winter dominated by strong trade winds . The climate of all sites generally follows this pattern, with some exceptions mentioned in the following paragraphs.

The Maido site, Reunion Island, is the site of the Maido Atmospheric Observatory (Baray et al., 2013). This site has been instrumented to perform UV measurements since February 2020 with a Kipp and Zonen SUV-E radiometer. This site has the advantage of being highly multi-instrumented; in situ measurements of the composition of the atmosphere are carried out (CO_2, CO, CH_4, etc.), meteorological measurements, and measurements of atmospheric profiles of temperature, water vapour or ozone (via lidar or radiosoundings). This site is located at 2200 m a.s.l.; outside the boundary layer, the environment is mountainous and uninhabited, and the climate is generally dry. The vegetation is sparse and consists of lichens and small shrubs, and the soil is composed of lapilli (Strasberg et al., 2005). This area is classified as shrubland on lapilli. This area has often been affected by fire episodes.

Table 1. Stations of the UV-Indien project. Date format is year/month.

Station	Location	Coordinates	Instrument	Data since	Frequency	UTC+	Altitude (a.s.l.)	Environmental conditions
Saint-Denis	Reunion	20.902° S 55.485° E	Bentham DTMc 300	2009/01	15 min	+4	82 m	Urban Coastal
			Radiometer Kipp and Zonen UVS-E-T 15-0124	2016/12	5 min			Low/middle pollution Tropical climate
			All-sky camera SkyCam Vision	2019/09	1 min			
Maido	Reunion	21.079° S 55.383° E	Radiometer Kipp and Zonen SUV-E 18-0020	2020/02	1 min	+4	2200 m	Rural Mountain
Anse Quitor	Rodrigues	19.758° S 63.368° E	Radiometer Kipp and Zonen UVS-E-T 16-0158	2017/06	1 min	+4	32 m	Rural Coastal
			All-sky camera SkyCam Vision	2019/09	1 min			No pollution Dry tropical climate
Mahé	Seychelles	4.679 ° S 55.531 ° E	Radiometer Kipp and Zonen UVS-E-T 17-0207	2017/11	5 min	+4	15 m	Semi-urban Coastal No pollution Tropical climate
Antananarivo	Madagascar	18.916° S 47.565° E	Radiometer Kipp and Zonen UVS-E-T 16-0159	2016/12	5 min	+3	1370 m	Urban Plateaux
			All-sky camera SkyCam Vision	2019/04	1 min			Middle/high pollution Tropical climate
Diego Suarez	Madagascar	12.279° S 48.287° E	Radiometer Kipp and Zonen SUV-E 18-0028	2019/11	1 min	+3	35 m	Semi-urban Coastal No pollution Tropical climate
Fort Dauphin	Madagascar	25.028° S 46.995° E	Radiometer Kipp and Zonen SUV-E 18-0030	2020/01	1 min	+3	10 m	Semi-urban Coastal
			All-sky camera SkyCam Vision	2020/01				No pollution Tropical climate
Moroni	Comoros	11.708° S 43.247° E	Radiometer Kipp and Zonen SUV-E 18-0027	2019/12	1 min	+3	12 m	Semi-urban Coastal
			All-sky camera SkyCam Vision					Low pollution Tropical climate
Ile Juan de Nova	France	17.054° S 42.711° E	Radiometer Kipp and Zonen SUV-E 18-0029	2019/04	1 min	+3	10 m	Small desert island Coastal No pollution Tropical climate

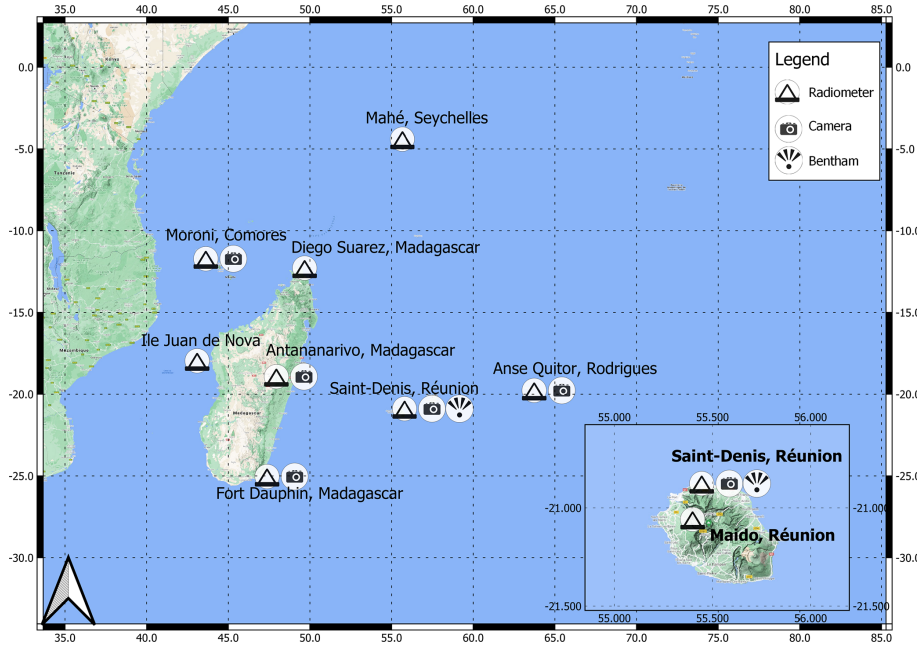

Figure 1. Location of the UV-Indien stations.

The site at Anse Quitor, Rodrigues, has been operational since June 2017 for UV measurements using a Kipp and Zonen UVS-E-T radiometer, and since September 2019 for cloudiness measurements. This site is located at 32 m a.s.l. near the coast, the climate is very dry, rainfall is low for most of the year, vegetation is sparse, and the terrain is slightly mountainous. The Mahé, Seychelles, site has been operational since November 2017 for UV measurements using a Kipp and Zonen UVS-E-T series radiometer. Cloudiness measurements are not yet possible as the deployment of the network has been delayed by the COVID-19 health crisis. The instrumented site is located at 15 m a.s.l. near the coast. The instrument is positioned at Victoria International Airport in an urban area. The island of Mahé has an equatorial climate all year round as it is located very close to the Equator. The vegetation of the instrumented area is sparse and consists of grasses and small shrubs and can be classified as savanna (Hume et al., 2013).

The site in Antananarivo, Madagascar, has been operational since December 2016 for UV measurements using a Kipp and Zonen UVS-E-T series radiometer. Cloudiness measurements are available from April 2019 onwards. The instrumented site is located at 1370 m a.s.l. in the highlands of Madagascar. Located in a densely populated urban area, the air quality of the site can be very degraded, and frequent pollution peaks are observed, as well as the presence of smog (Gorremans and Masquelier, 2018). The radiometer and camera are installed on the roof of the Geophysical Institute and Observatory of Antananarivo (IOGA).

The instrumental site of Diego Suarez, Madagascar, has been equipped with a Kipp and Zonen SUV-E radiometer since November 2019, and the deployment of the camera there has been delayed due to technical incidents following the passage of tropical cyclone Belna and due to the recent health crisis. The site is located at an altitude of 35 m a.s.l. close to the coast in a semi-urban area where air pollution is generally low.

The site of Fort Dauphin, Madagascar, has been equipped with a Kipp and Zonen SUV-E radiometer and a SkyCam Vision camera since January 2020. This site is very similar to the one in Diego-Suarez: it is located at an altitude of 10 m a.s.l. close to the coast in a semi-urban area where air pollution is generally low. However, there is a 10° latitude difference between this site and Diego-Suarez.

The site of Moroni, Comoros, has been equipped with an SUV-E radiometer and a SkyCam Vision camera since December 2019. The instruments are located on the roof of the Agence Nationale de l'Aviation Civile et de la Météorologie des Comores and are therefore co-located with meteorological records of rainfall and temperature. The site should soon be equipped with a SAOZ that will allow for the monitoring of the total ozone column. The site is located at an altitude of 12 m a.s.l. in an urban area and close to the coast where the air is generally not very polluted.

Juan de Nova Island is located in the centre of the Mozambique Channel, it is an integral environmental reserve, and its access is strictly regulated. There are no inhabitants on this island. This site has been equipped with a Kipp and Zonen radiometer since April 2019. The purchase of the equipment and its installation were supported by the French space agency (CNES), which is very interested in this type of data for the validation of satellite sounders. Access to this island

is difficult, and data are stored there but can only be retrieved locally, so they are brought back at least only once a year. However, this was not the case during the recent health crisis. This completely flat coral desert island has an area of 4.80 km^2 with very sparse vegetation. The instrumented site is at an altitude of 10 m a.s.l.

3 Instrumentation and data

3.1 UV-Indien instrumentation

Each station in the UV-Indien network is equipped with at least one broadband UV radiometer. This is usually supplemented by an all-sky camera. The radiometers installed at the UV-Indian Network sites are the Kipp and Zonen UVS-E-T or the Kipp and Zonen SUV-E. The camera installed is a SkyCam Vision developed by Reuniwatt. Some stations of the UV-Indian Network are on the same site as other measurement networks (NDACC, ICOS, AERONET, etc.) and therefore benefit from more complementary measurements. The specificities of the instruments of the UV-Indien network only will be detailed here, namely the radiometers and the camera.

3.1.1 Instrument details

The Kipp and Zonen UVS-E-T radiometer is a radiometer designed to have a spectral response close to the erythemal action spectrum (ISO 17166:1999/CIE S 007/E-1998). The detection system consists of an optical filter and a phosphor, which determines the spectral response. The phosphor, sensitive to UV light, emits light which is then detected by a photodiode. The resulting signal is amplified, and the output voltage, multiplied by 40 $m^2\,W^{-1}$, gives an estimate of the UVI. The angular response of the radiometer is a function of the cosine of the zenith angle. According to the manufacturer, the expected daily uncertainty is less than 5 %, the measurement drift of the sensor is less than 5 % per year, the directional response error is less than 2.5 %, and the non-linear error is less than 1 %. The Kipp and Zonen SUV-E is the new version of the UVS-E-T from the same manufacturer. This new radiometer no longer has a desiccant that needs to be changed regularly and has a digital interface. It is also designed to have a spectral response close to the erythemal action spectrum (ISO 17166:1999/CIE S 007/E-1998). Its detection system is similar to that of the Kipp and Zonen UVS-E-T. The expected daily uncertainty, according to the manufacturer, is less than 5 %. The measurement drift of the sensor is less than 5 % per year, its directional response error is less than 5 $m^2\,W^{-1}$, and its non-linear error is less than 1 %. The broadband radiometers are calibrated about every 2 years (depending on logistical and current health conditions) according to a procedure that is specified in Sect. 3.1.2. The SkyCam Vision camera built by Reuniwatt is an all-sky camera that acquires hemispheric images of the sky in the visible spectrum every minute. The CMOS acquisition sensor has a resolution of 2048 × 2048 pixels, and the acquisition frequency is usually 30 s but can be modified. The cloud fraction calculated by the camera is obtained according to the ELIFAN algorithm, developed at CNRS (Centre National de la Recherche Scientifique), France (Lothon et al., 2019). The algorithm is based on the application of criteria and thresholds on the distribution of R / B ratios and the R / B ratio of each pixel. Two treatments are performed: an "absolute" treatment and a "differential" treatment with respect to a library of clear-sky images built up initially. The steps of the process are as follows:

- limitation of the processed image contour;
- application of masks: solar and object;
- detection of clear-sky and fully cloudy images;
- discrimination between clear-sky and fully cloudy images through an absolute or differential threshold process.

More information on this camera is available on the manufacturer's website, http://www.reuniwatt.com/ (last access: 19 August 2021), and in Lothon et al. (2019) for the ELIFAN algorithm. The Bentham DTMc300 spectrometer consists of a dual monochromator giving irradiance measurements with a wavelength step of 0.5 nm and a full width at half maximum of 0.5 nm. The measurements are cosine corrected, temperature stabilised, and calibrated every 3 months with standard 1000 W lamps that can be traced back to the National Institute of Standards and Technology. This instrument also underwent intercomparison during a QASUME (Quality Assurance of Ultraviolet Measurements in Europe) campaign in 2013. The Bentham used in the UV-Indien network, located in Saint-Denis de la Réunion, Moufia site, showed a bias of about 3 % (Bentham measurements lower than measurements with the reference instrument). The uncertainty on irradiance is about 5 % for a coverage factor of $k = 2$ (Brogniez et al., 2016).

3.1.2 Maintenance and calibration protocols

The radiometers do not require any particular maintenance except a regular cleaning of the dome. For older models of the Kipp and Zonen radiometer (Kipp and Zonen UVS-E-T), it is also necessary to change the desiccant approximately every 6 months or when necessary (colour change). This is done by our local partner. In general, it is usual to recalibrate this type of radiometer every 2 years to avoid drift. The calibration protocol is identical for the UVS-E and SUV-E radiometers. However, this protocol depends on the type of radiometer and the type of calibration most recently performed for each radiometer. Table 3 shows the last calibration performed for each radiometer. There are three types of calibration: the manufacturer's calibration, the PMOD/WRC

(World Radiation Centre in Davos, Switzerland, and World Radiation Center) calibration named Davos calibration hereafter, and the Bentham calibration. The manufacturer's calibration is used from the start of the instrument's operation and for a period of approximately 2 years. This period can be extended to 3 years when logistical constraints do not allow the recovery of the radiometer at its installation site. It should be noted that many of the stations in the network are costly to transport and are located in countries and regions that are difficult to access, with little or no freight service. Even though this calibration step is essential for the quality of the measurements, we have to adapt our constraints. The manufacturer's calibration is a function of the solar zenith angle and the total ozone column. This calibration is performed with a xenon lamp, a monochromator (Oriel Cornerstone MS257), and a sensor consisting of a calibrated silicon photodiode. The calibration coefficient is obtained following several monochromatic measurements from 280 to 400 nm with an increment of 1 nm. In order to take both the actual response of the instrument and the ideal response into account, a radiative transfer model is used to estimate the sensitivity as a function of several atmospheric spectra corresponding to zenith solar angles ranging from 0 to 70° in 5° steps and from 260 to 400 DU (Dobson unit) in 10 DU steps. When the manufacturer's calibration expires, the instrument is recalibrated in two different ways. If our budget can cover the cost, the instrument is sent to the World Radiation Centre in Davos, Switzerland (PMOD). Otherwise, it is recalibrated directly on the Moufia station in Reunion Island by direct comparison with the calibrated values of the Bentham spectroradiometer. The calibration performed at the PMOD/WRC is carried out in three steps, allowing the weighted irradiance to be calculated according to the following formula:

$$E_{\mathrm{CIE}} = (U - U_{\mathrm{offset}}) \cdot C \cdot f_n(\mathrm{SZA}, \mathrm{TOZ}) \cdot \mathrm{coscor}.$$

U is the value of the raw voltage signal of the radiometer. The calibration therefore allows the following four parameters to be determined:

- C, the absolute calibration factor determined for a solar zenith angle, SZA, of 40° and total column ozone (TO3) of 300 DU
- the conversion function (normalised), f_n, which converts from the detector weighted solar irradiance to erythemal weighted irradiance
- coscor, a factor that corrects the detector cosine error
- the dark offset, U offset, which is determined every night.

More details are available at https://www.pmodwrc.ch/en/world-radiation-center-2/wcc-uv/uv-radiometer-calibration-services/ (last access: 19 August 2021).

The Bentham calibration consists of co-locating the radiometers with the Bentham DTMc300 at the Saint-Denis site for a period of 3 to 4 months. The relative differences between the radiometers and the Bentham measurements are then calculated and are also classified by SZA band (about ±5°). The average of these relative difference bins allows us to obtain a calibration coefficient depending on the SZA. The average of all relative differences (without distinction of SZA) is also calculated to obtain an average calibration coefficient. This calibration could be refined by also classifying the biases according to the total ozone column observed during the measurement, but this has not been done. In order to obtain sufficient measurement points covering all observed total ozone column values in the Indian Ocean region, the intercomparison period would need to last at least 1 year to capture the annual ozone cycle. A period of 1 year is too long for the capabilities and needs of the Indian UV network, and therefore the Bentham calibration does not include the total ozone column discrimination. The use of a transfer model could also overcome this shortcoming.

A Bentham calibration was performed for the UVS-E-T 15-0124 and SUV-E-1800 (27/28/29/30) radiometers between June 2019 and December 2019, and average relative differences ranging from about −10 % to +5 % were obtained before recalibration. The SUV-E radiometers (previously calibrated by the manufacturer) tend to underestimate the UVI (by about 10 %) with respect to the Bentham measurements. The UVS-E-T 15-0124 radiometer (recalibrated DAVOS-PMOD/WRC) tends to overestimate UVI by about 3 % compared to the Bentham measurements. The relative differences depend on the SZA and tend to become more pronounced as the SZA increases. After recalibration of the UVS-E-T and SUV-E radiometers using the calibration coefficients described above, a second comparison with the Bentham measurements showed average relative differences of ±4 %.

Although the Bentham calibration does not directly take into account the total ozone column, it has been established from the measurements of the recalibrated radiometers by the manufacturer, and this manufacturer calibration does take into account the total ozone column. The impact of this shortcoming of the Bentham calibration has not yet been studied in detail by our teams. Nevertheless, no significant offset has been observed for the moment in the data series following a Bentham recalibration. The future recalibration of the oldest radiometers will allow us to investigate these questions further. An update of the dataset is therefore to be expected, which will of course be accompanied by versioning and detailed documentation of the changes. The cameras do not require any particular maintenance except for regular cleaning of the window.

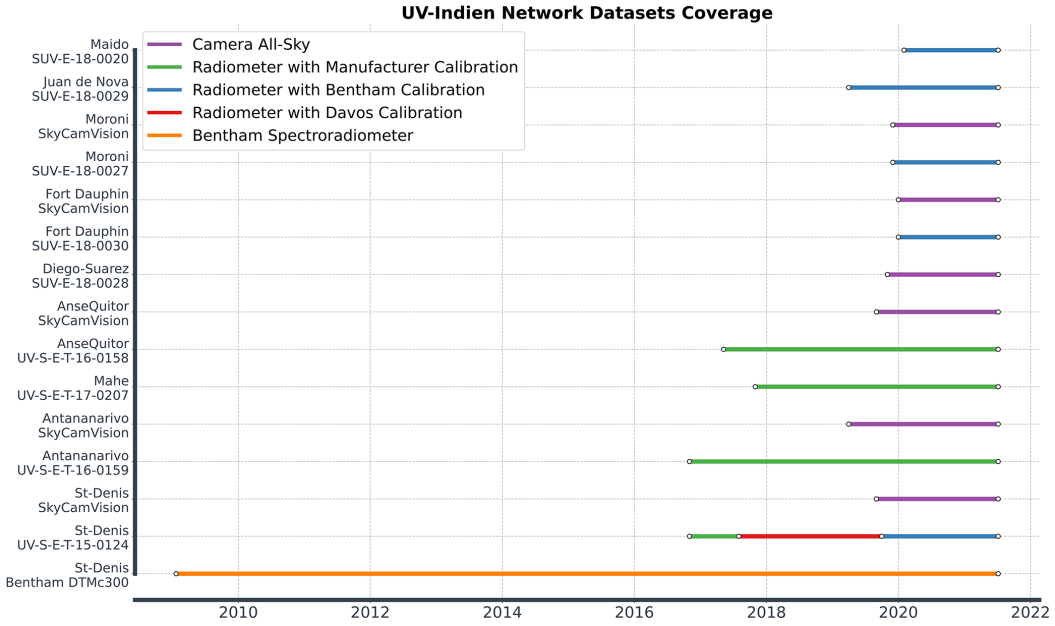

Figure 2. Timeline of the instruments of the UV-Indien network. The measurement periods of the cameras are shown in purple. The measurement period of the Bentham spectroradiometer is shown in orange. The measurement periods of the radiometers that are either manufacturer-calibrated, Davos-calibrated, or Bentham-calibrated are shown in green, red, and blue, respectively.

3.1.3 Data processing

With the exception of the station on the island of Juan de Nova, raw data are transmitted daily. These data then undergo a first processing stage in which a first quality control eliminates acquisition errors or outliers. The raw data files are in different formats depending on the station and its method of data acquisition and transfer. They are therefore converted into a single format before recalibration. Depending on the most recent calibration of the instrument, the data are recalibrated according to the manufacturer's calibration procedure: Davos or Bentham. They are then reformatted in the format requested by the various distribution platforms (WOUDC or Zenodo). The frequency of updating the online databases is 3 to 6 months. For the Juan de Nova station, an annual rotation is planned in order to physically recover the data and carry out the maintenance of the instrument. The radiometer data are filtered to define the UVI measurements made in clear skies. This filtering is done manually for 1 h intervals. The filtering process is as follows: each daily UVI and cloud fraction profile is plotted, together with an estimate of the clear-sky profile, using the Madronich analytical formula (Madronich, 2007). To calculate the Madronich UVI estimate, we use the total ozone column from either the OMTO3d satellite product or a co-located ground-based instrument (the SAOZ for the Saint-Denis station). An observer then selects the 1 h windows considered as clear sky according to the following criteria:

- Difference between observed and estimated UVI (according to the Madronich analytical formula) is higher than 10 %.
- For the presence of clouds, a cloud fraction threshold of 0.25 is set.
- For the shape and regularity of the UVI curve during the day, a Gaussian (or semi-Gaussian) curve indicates a day (or half-day) not affected by the presence of clouds. As clouds generally have a high temporal variability, rapid development of clouds usually results in rapid variations in UVI over a few minutes.
- Cloud cover can also be quasi-homogeneous and quasi-constant over the day, which does not lead to sudden variations in UVI. This case is also excluded from the filtering.

Figure 2 represents the time period covered by all the instruments of the UV-Indien network and their respective calibrations.

4 Data overview

4.1 Diurnal variation in UVR and CF

For each station, the variability in the UV index, as measured by the radiometers, was analysed to understand the variability in the dataset and ensure its quality. The diurnal cycle of UVI was calculated from the start of measurements at

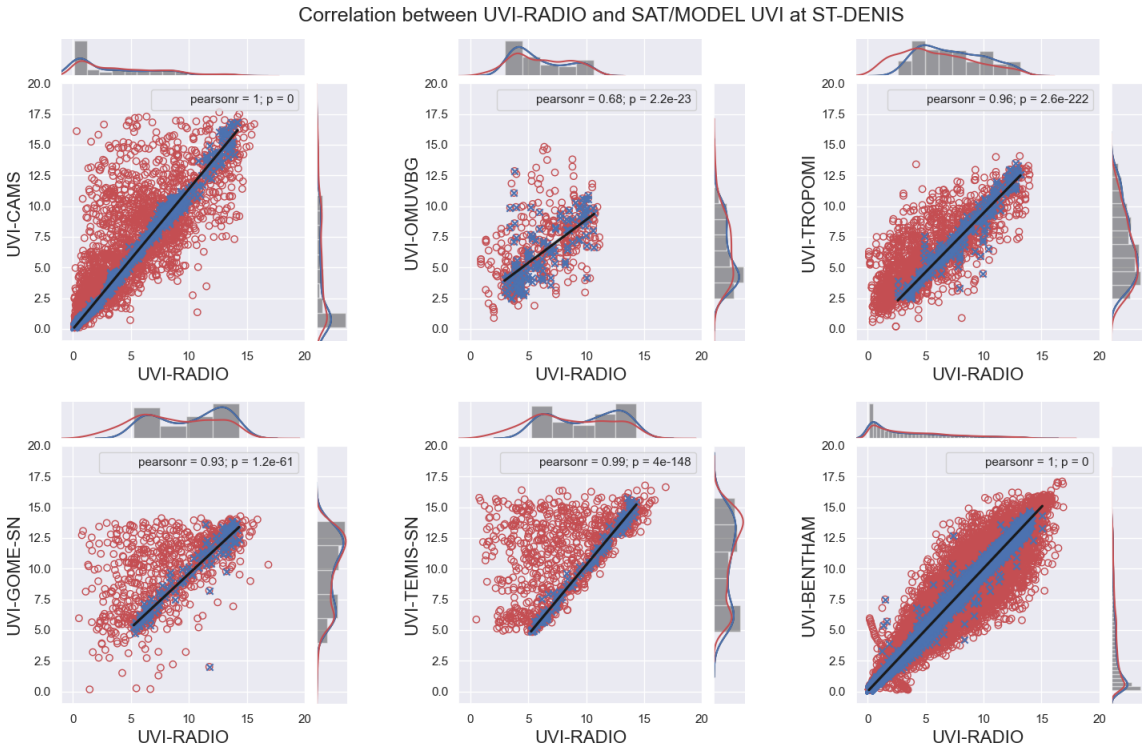

Figure 3. Correlation between UVI-RADIO and satellite/model estimates at Saint-Denis. A histogram representing each dataset distribution is represented at the right and at the top side of each subfigure. The clear-sky measurements made by UVI-RADIO have been distinguished and are shown as blue crosses, while the measurements for all-sky conditions are shown as red circles.

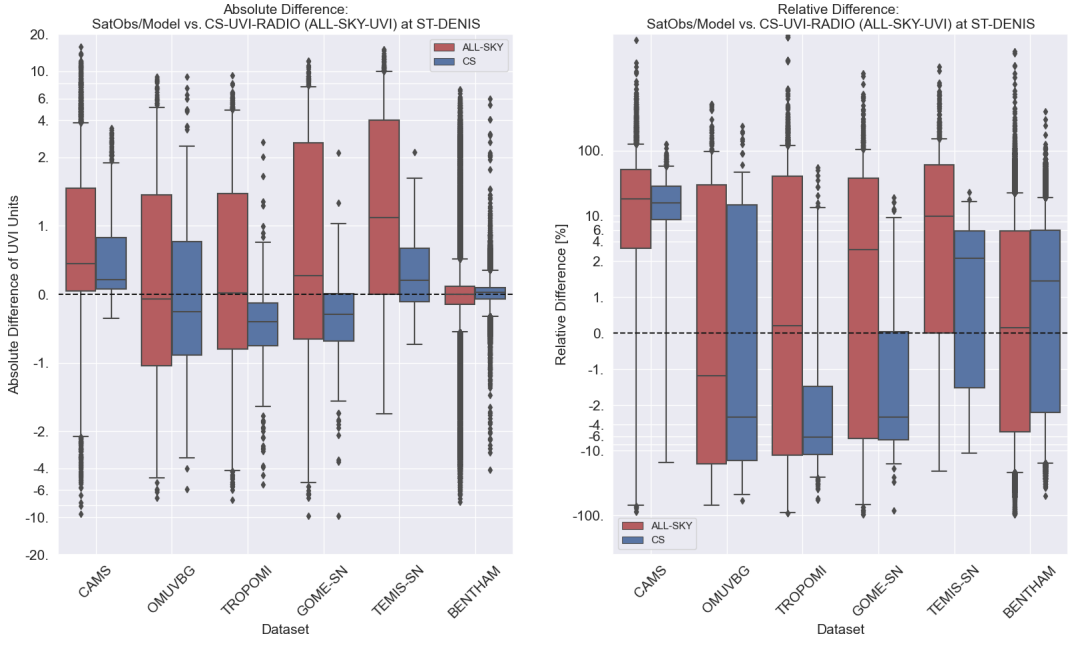

Figure 4. Boxplot of differences between UVI-RADIO and satellite/model estimates at Saint-Denis.

each station until June 2020 for Anse Quitor, November 2020 for Mahé, and December 2020 for Antananarivo and Saint-Denis. The results are presented in Fig. 5: the mean UVI (blue line), the UVI maximum (continuous red line), and the first and third quartiles (blue shading) of the UVI in all-sky conditions during the day are represented for Antananarivo, Mahé, Anse Quitor, and Saint-Denis. For a given station, in clear-sky conditions, the mean UVI is represented by a green line, the maximum UVI by a dashed red line, and quartiles by shades of green. In all-sky conditions, the mean UVI at local solar noon varies from about 10 (Antananarivo, Anse Quitor, Saint-Denis) to about 14 (Mahé). The difference between Mahé and the other three stations can be explained by the latitudes of the stations: Antananarivo, Anse Quitor, and Saint-Denis are at about 20° S, while Mahé is at 4.6° S. Therefore, in Mahé, SZAs are lower throughout the year, which induces a higher UVI during the year. For clear-sky conditions, the mean UVI is higher than for all-sky conditions at all stations. In addition, the first and third quartiles are closer to the mean in clear-sky conditions. This is due to the impact of cloud attenuation on UVI variability. It can be seen that the UVI maxima can be higher than 20 for Anse Quitor, Antananarivo, and Mahé. For Saint-Denis, the UVI maxima can reach 16. The highest UVIs are observed at the Mahé station with maxima of up to 25. At all stations, the UVI maxima are higher for all-sky conditions than clear-sky conditions. These maxima of UVI in all-sky conditions can be 1 to 4 units of UVI higher than maxima in clear-sky conditions. This is due to the enhancement of UVI by fractional cloud cover, which can produce multiple scattering, thus enhancing the UVI on the surface. This phenomenon was previously observed at Saint-Denis (Lamy et al., 2018) and has been described in past studies for other regions of the world (Badosa et al., 2014; Sabburg and Wong, 2000). The largest differences between the maxima in all-sky conditions and clear-sky conditions are observed at Mahé, and the smallest differences are observed at Saint-Denis and Anse Quitor. Antananarivo also shows a significant absolute increase in UVI by about 2 to 3 units. Antananarivo is at a higher altitude than the other three stations, at about 1.3 km a.s.l. The city is also located inland and suffers from heavy pollution. Therefore, both aerosols and altitude can be expected to have a significant impact on the variability in surface UVIs. In Antananarivo, the peaks of UVI mean and maxima are aligned for both clear-sky and all-sky conditions. In Saint-Denis the peak of mean UVI occurs later in the day for clear-sky conditions than for all-sky conditions. In Anse Quitor, the peak of UVI is early in the day. This is due to the time zone used at Anse Quitor. Rodrigues Island, where Anse Quitor is located, shares the same time zone as Saint-Denis (Reunion Island) and Mahé (Seychelles) but is farther east by about 8° of longitude. In Mahé, the peaks of mean UVI, in all-sky and clear-sky conditions, are aligned. This is not the case for the maxima, which occur 1 to 2 h earlier in all-sky conditions than in clear-sky conditions. The position of the UVI peaks can be explained by the variability in the cloud cover, as will be shown in the next section. The monthly averages of the daily UVI maximum and the daily UVI at solar noon have also been calculated. Although the datasets do not cover a sufficient period to be climatologically significant, the annual variability and the differences between UVI and UVI daily maxima at solar noon present interesting results. Figure 6 shows these monthly averages for the four stations of Antananarivo, Saint-Denis, Mahé, and Anse Quitor. The measurement periods used to obtain these monthly averages were the same as for Fig. 5. The daily maxima of UVI are in red lines with filled circles, and the corresponding sun zenith angles are in dashed orange lines with filled circles. The UVIs at local solar noon are marked with blue lines and crosses, and the corresponding sun zenith angles are shown as dashed orange lines with crosses. For all stations and all months of the year, the maximum daily UVI (UVI_{DMAX}) is higher than the average UVI at solar noon (UVI_{SNOON}). These monthly averages are based on datasets for all types of cloud cover. Thus, the cloud cover will introduce a bias in the result. UVI_{DMAX} includes maxima of UVI during cloud enhancements, which could occur earlier or later than the local solar noon, as discussed in the previous result (Fig. 5). UVI_{DMAX} also includes maxima of UVI during clear-sky days, which will usually occur at local solar noon. UVI_{SNOON} will include only UVI at local solar noon with or without cloud cover. This is why UVI_{DMAX} is always higher than UVI_{SNOON} in all-sky conditions. The differences range between 1 during austral winter at Saint-Denis and 6 in austral summer at Mahé. The corresponding SZA differences range from 0 to 6°. Looking at the few complete clear-sky days revealed a UVI_{SNOON} and a UVI_{DMAX} that were almost equivalent. However, as there were not enough clear-sky measurements per month and per SZA bin, these results are not represented here.

4.2 Seasonal distribution and variation in UVR and CF

Early results from the cameras provide a brief description of the mean diurnal cloud cycles over each station. Figure 7a shows the mean diurnal cycle of the cloud fraction (CF) over Antananarivo for the entire year (black curve), along with the distribution of the first and third quartiles (blue shaded areas). Seasonal means of CF are also presented for December, January, and February (DJF, in green), March, April, and May (MAM, in red), September, October, and November (SON, in orange), and June, July, and August (JJA, in purple). The density of the corresponding dataset for each month of the year is represented in Fig. 7b. Figure 7c represents the difference of UVI maxima between clear-sky UVI (CS-UVI) and all-sky UVI for the same period. The UVI distribution is also available in Fig. 7d. The same results are presented for Saint-Denis in Fig. 8. Over Antananarivo (Fig. 7), the annual mean diurnal cycle shows intermediate values of CF of about 0.6 at the beginning of the day. CF tends to decrease during the day and to increase in the late afternoon. Antana-

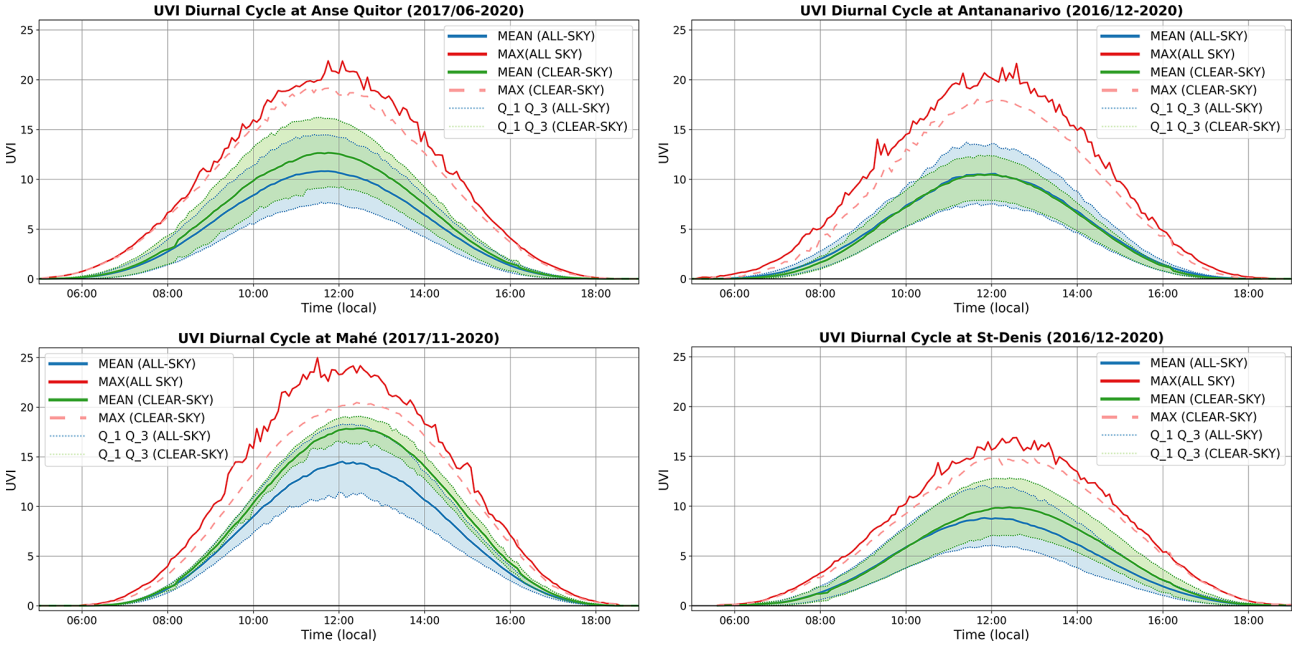

Figure 5. Diurnal cycle of UVI at Anse Quitor, Antananarivo, Mahé, and Saint-Denis. In all-sky conditions, mean UVI is in blue, max UVI is in red, and first and third quartiles delimit the blue shaded area. In clear-sky conditions, mean UVI is in green, max UVI is in dashed red, and first and third quartiles delimit the green shaded area.

narivo is located in a mountainous region in the highlands of Madagascar at 1370 m a.s.l. The difference in CF in the four seasons is not statistically significant, especially for the JJA and SON seasons. Since the camera at Antananarivo was installed in April 2019, there are not yet significant numbers of data points for certain months of the year. Nonetheless, since the radiometer at Antananarivo was installed in 2016, there is a significant number of UVI data over the whole year (Fig. 7d). The largest difference between maxima of UVI in clear-sky conditions and maxima of UVI in all-sky conditions can be observed for the DJF and JJA seasons (Fig. 7c). The diurnal CF profiles show a slightly higher CF over a large part of the day in the JJA season compared to the annual profile or the other seasons. The CF diurnal cycle alone is probably not the only factor involved in triggering UVI enhancement: cloud distributions and type of clouds probably play a role (Sabburg and Wong, 2000; Calbó et al., 2005; Badosa et al., 2014). The measurements proposed here will be fully useful in carrying out this type of study.

Over Saint-Denis the mean diurnal CF cycle shows a different profile from that of Antananarivo. CF values are lower in the morning, at around 0.4, and increase during the day to reach 0.6. Saint-Denis is located on the northern part of Reunion Island, a mountainous island under the influence of the south-east trade winds which induce cloud formation on the southern part of the island during the morning. During the day, the clouds tend to overflow over the rest of the island, thus inducing a rising CF during the day. The lowest values of CF throughout the day are observed in SON. DJF, MAM, and JJA follow the annual mean. For this station, well-spread CF and UVI data are available throughout the year (Fig. 8b and d). A glance at the difference between the maxima of UVI in clear-sky conditions and the maxima of UVI in all-sky conditions (Fig. 7c) shows that almost all the highest differences are observed for the DJF season. These differences can reach −2.4. The JJA season also shows large differences during the morning, but, after 10:00 (for time zones, see Table 1), the differences are smaller than in DJF most of the time. CF also starts to increase faster from 10:00 onwards for the JJA season. (Fig. 7a). This result could indicate that UVI enhancement occurs less frequently above a certain CF threshold. The cameras of the UV-Indien network present promising results for studying cloud variability and its impact on UV radiation in the Indian Ocean region. CF alone is probably not sufficient to give an understanding of UVI enhancement. Cloud types, types of cloud distribution, and solar occultation by clouds also need to be considered. Moreover, the UV-Indien network is just starting up, so there is not yet enough data for significant climatological studies to be conducted.

The statistics obtained on the diurnal cycles of the UVI show consistent results, the maxima measured by the radiometers do not seem to be outliers but rather the consequence of physical phenomena such as the increase in radiation by clouds. The monthly averages of daily UVI maxima and UVI measured at solar noon at the four sites of Antananarivo, Saint-Denis, Mahé, and Anse Quitor are consistent with the variation in the zenith solar angle at these differ-

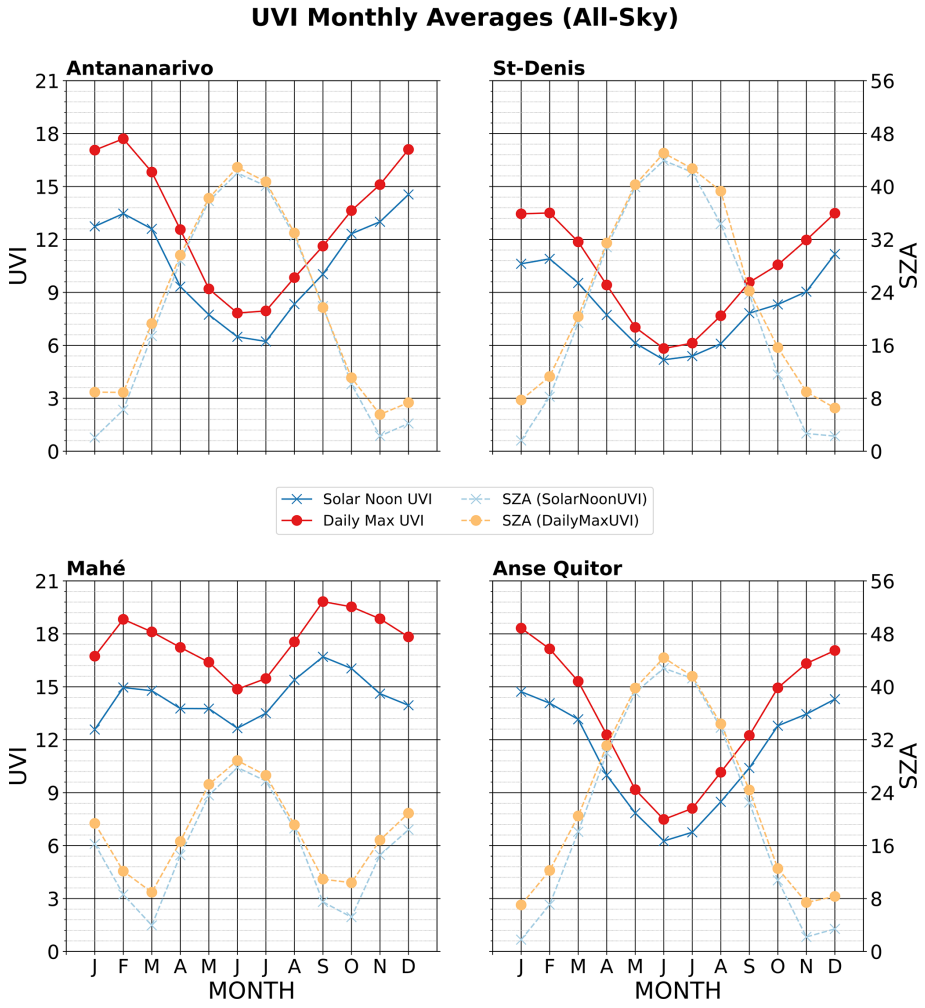

Figure 6. UVI monthly averages in all-sky conditions for the four stations of Antananarivo, Saint-Denis, Mahé, and Anse Quitor. The monthly averages of the daily max UVI is represented by the red line with filled circles. The corresponding SZA is represented by the dotted orange line. The monthly averages of the UVI at solar noon is represented by the blue line with blue crosses. The corresponding SZA is represented by the dashed blue line.

ent sites. For the Antananarivo and Saint-Denis sites, coherent behaviour is observed between the all-sky camera measurements and the radiometer measurements over the whole dataset or over the four seasons represented here.

4.3 Comparison against existing UVI product

4.3.1 Other UVI estimates available in the Indian Ocean region

UVI ground-based observations offer high temporal and spectral resolution and precision. However, to study the impact of climate change on the UVI, global estimates of UVI are also needed. Satellites and global forecast models provide such estimates. To compute the UVI at the surface, the global forecast model uses a radiative transfer model (RTM) or a look-up table generated by an RTM. Multiple parameters are required, such as TOC, aerosols, CF, and SZA. To determine the UVI at the surface, satellite UV estimates are calculated using a combination of RTM calculations and measurements. In order to compare ground UVI measurements with the UVI product from satellites or forecast modelling, we have gathered together the multiple datasets presented in Table 2.

The Bentham spectrometer (called UVI-BENTHAM hereafter) and Kipp and Zonen radiometer (called UVI-RADIO hereafter) constitute the ground-based-instrument part of the UV network. These instruments will be compared with satellite surface UV products – TROPOspheric Monitoring Instrument (TROPOMI), OMUVBG, and Global Ozone Monitoring Experiment (GOME-2) – and forecast model products – Copernicus Atmospheric Monitoring Service (CAMS) and Tropospheric Emission Monitoring Internet Service (TEMIS).

The TROPOMI instrument is on board the Sentinel-5 Precursor (S5P) polar-orbiting satellite launched on 13 October

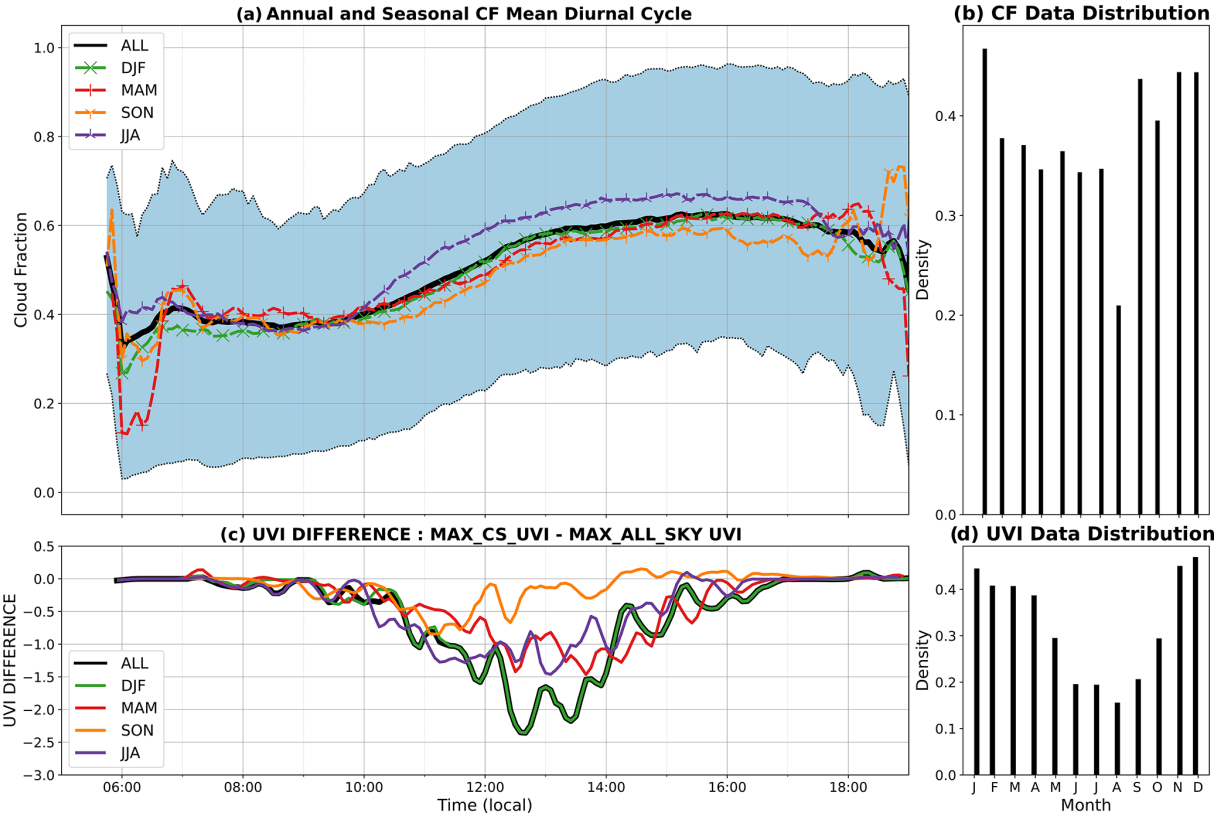

Figure 7. **(a, b)** Diurnal cycle of CF at Antananarivo. Annual mean CF is in black, and first and third quartiles delimit the blue shaded area. Seasonal mean is in green (DJF), red (MAM), orange (SON), and purple (JJA). **(c, d)** Diurnal cycle of the difference between maxima of UVI in clear-sky conditions and in all-sky conditions at Antananarivo. Annual max UVI differences are in black. Seasonal max UVI differences are in green (DJF), red (MAM), orange (SON), and purple (JJA)

2017 as part of the EU Copernicus programme. TROPOMI surface UV radiation products include irradiances with daily integrals at four different wavelengths and dose rates with daily doses for erythema (CIE Standard, 1998) and vitamin D synthesis (Bouillon et al., 2006) action spectra. All parameters are calculated for overpass time, solar noon time, and clear-sky conditions (no clouds, no aerosols). Details of the TROPOMI algorithm can be found in Lindfors et al. (2018), Garane et al. (2019), and Arola et al. (2009). The ground resolution for the UV products is $7.2 \times 3.5\,km^2$ ($5.6 \times 3.5\,km^2$ since 6 August 2019) at nadir. Only the estimates corresponding to the time of the overpass are chosen here. The UVI estimated in clear-sky conditions and in all-sky conditions will be used in this study and will both be called UVI-TROPOMI for ease of reading. UVI-TROPOMI computed for clear-sky conditions will be compared against UVI-RADIO or UVI-BENTHAM measured in clear-sky conditions, and UVI-TROPOMI computed for all-sky conditions will be compared against UVI-RADIO or UVI-BENTHAM measured in clear-sky conditions.

OMUVBG is a product derived from the Ozone Monitoring Instrument (OVI) (Levelt et al., 2006; Tanskanen et al., 2007; Arola et al., 2009). It is based on the Total Ozone Mapping Spectrometer (TOMS) algorithm to retrieve TOC. An RTM is used along with TOC, climatological albedo, ozone and temperature profile, elevation, SZA, and cloud modification factor to estimate the UVI in all-sky conditions (called UVI-OMUVBG hereafter). This estimate corresponds to the satellite overpass time. Detailed information on this product is available in Tanskanen et al. (2006) and Tanskanen et al. (2007). UVI-OMUVBG computed for clear-sky conditions will be compared against UVI-RADIO or UVI-BENTHAM measured in clear-sky conditions, and UVI-OMUVBG computed for all-sky conditions will be compared against UVI-RADIO or UVI-BENTHAM measured in clear-sky conditions.

The offline surface UV is a product derived from the measurements of the GOME-2 instruments on board the MetOp-B and MetOp-C satellites. The offline surface UV contains multiple variables related to UV radiation and human health: UVI, integrated UVB and UVA, and daily doses derived from different biological weighting functions (erythema, DNA damage, plant damage, and vitamin-D synthesis). TOC and cloud measurements provided by the Satellite Application Monitoring on Atmospheric Composition Monitoring (AC SAF) total ozone product and the Advanced Very High Res-

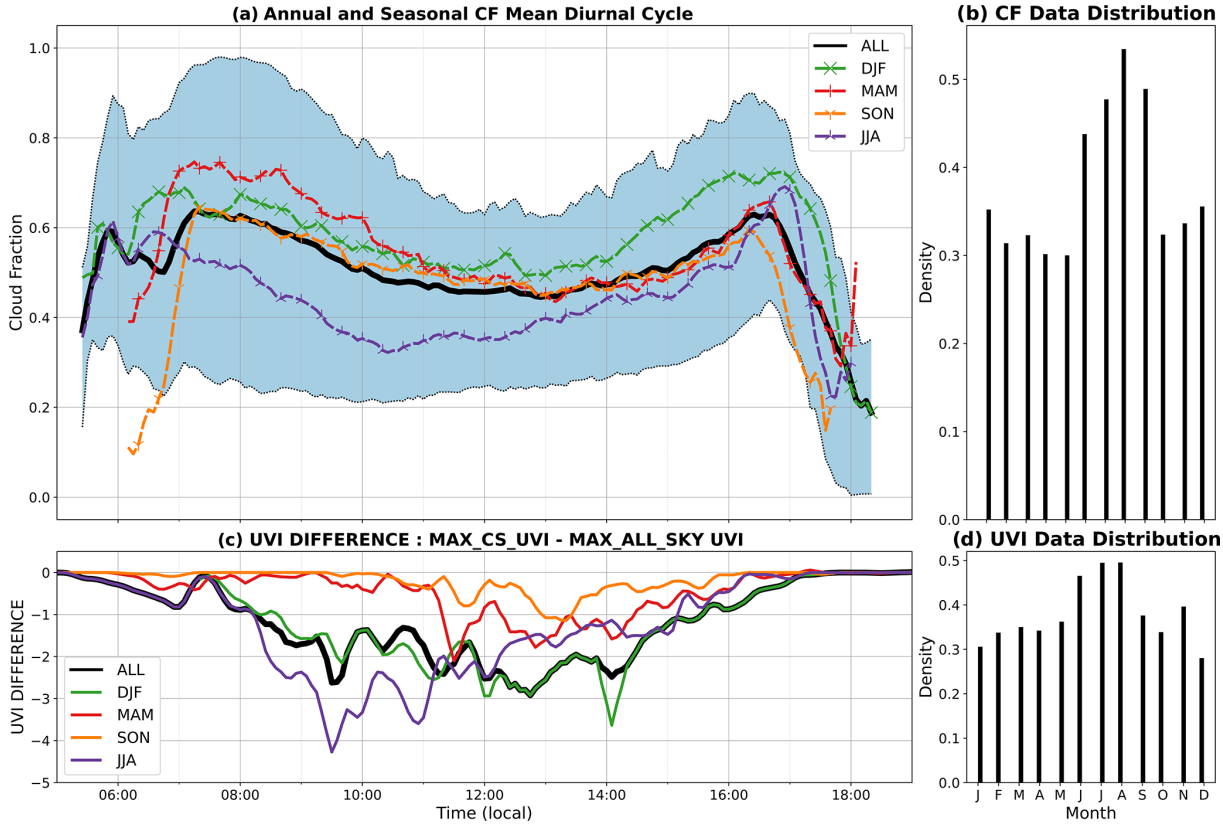

Figure 8. **(a, b)** Diurnal cycle of CF at Saint-Denis. Annual mean CF is in black, and first and third quartiles delimit the blue shaded area. Seasonal mean is in green (DJF), red (MAM), orange (SON), and purple (JJA). **(c, d)** Diurnal cycle of the difference between maxima of UVI in clear-sky conditions and in all-sky conditions at Saint-Denis. Annual max UVI differences are in black. Seasonal max UVI differences are in green (DJF), red (MAM), orange (SON), and purple (JJA).

olution Radiometer (AVHRR-3) reflectances are used with an RTM to compute the offline surface UV product (Kujanpää and Kalakoski, 2015). The product is given on a regular $0.5 \times 0.5°$ grid, and UVI is computed at local solar noon (called UVI-GOME hereafter).

The Integrated Forecasting System (IFS) of the Copernicus Atmosphere Monitoring Service (CAMS) has been providing UV forecasts since 2012 (Bozzo et al., 2015). More precisely, it provides the spectral UV with a spectral resolution of 5 nm and the UVI by integrating the spectral UV according to the erythema action spectrum (CIE Standard, 1998). The UV irradiances and UVI are produced in clear-sky and in all-sky conditions (hereafter called UVI-CAMS). For UVI-CAMS, new forecasts are available every 12 h. The model output has a time step of 3 h. From the first forecast of the day, which starts and is initialised at 00:00:00, we take the first, second, third, and fourth time steps of the model (00:00:00, 03:00:00, 06:000:00, and 09:00:00, respectively), and, from the second forecast which starts at 12:00:00, we take the first, second, third, and fourth time steps (12:00:00, 15:00:00, 18:00:00, and 21:00:00, respectively). The horizontal resolution was approximately 80 km prior to 21 June 2016 and approximately 40 km afterwards. Following its continuous development, the CAMS model has been upgraded every year with components that significantly change the UVI forecasts. For instance, improved handling of cloudiness (implemented on 24 January 2017) and a new extraterrestrial UV spectrum (implemented on 26 September 2017) have resulted in significant improvements (Pitkänen et al., 2020). As these changes only affect the data following the upgrade, the CAMS UV forecast is not a homogeneous time series but should be considered as an evolving UV product with which measurements can be compared. More information on the IFS and CAMS-IFS models is available at https://atmosphere.copernicus.eu/node/326 (last access: 19 August 2021). UVI-CAMS computed for clear-sky conditions will be compared against UVI-RADIO or UVI-BENTHAM measured in clear-sky conditions, and UVI-CAMS computed for all-sky conditions will be compared against UVI-RADIO or UVI-BENTHAM measured in clear-sky conditions.

The TEMIS UVI product is derived from the TOC at solar noon obtained by satellites (SCIAMACHY, GOME-2A, or GOME-2B depending on the time period). Following the

Table 2. Satellite, model, and ground-based data.

Dataset	Platform	Type	Resolution	Field used for computation/calibration		References
				Ozone field used	Aerosol field used	
Bentham	Ground-based	Spectrometer	$dt = 15$ min	None	None	Brogniez et al. (2016)
Radiometer K and Z (UVI-RADIO)	Ground-based	Radiometer	$dt = 1$ or 5 min	SAOZ or OMI	None	Cadet et al. (2020)
OMUVBG	Satellite	Spectrometer (measurement at 360 nm then table look-up)	Daily (overpass/ solar noon) $0.25 \times 0.25°$	OMI	OMI Krotkov et al. (1998) Herman et al. (2009)	Tanskanen et al. (2006) Arola et al. (2009) Levelt et al. (2006)
TROPOMI	Satellite	Spectrometer (measurement at 354 nm then table look-up)	Daily (overpass/ solar noon) 5.6×3.7 km	TROPOMI L2 total ozone column product (Garane et al., 2019).	Aerosol climatology Kinne et al. (2013)	Lindfors et al. (2018) Lakkala et al. (2020)
GOME	Satellite	Spectrometer	Daily (local solar noon) $0.5 \times 0.5°$	GOME-2A TOZ	MODIS Level 3	Kujanpää and Kalakoski (2015)
CAMS	Model	Modelling	$dt = 6$ h 40 km (after 21 June 2016) 80 km (before 21 June 2016)	Modelled	Modelled	Bozzo et al. (2015)
TEMIS	Model	Modelling	Daily (local solar noon) $0.5 \times 0.5°$	SCIAMACHY GOME-2A Multi-sensor reanalysis	No direct correction	Zempila et al. (2017)

Table 3. Radiometers of the UV-Indien network.

Radiometer	Current calibration type	Date of current calibration	Calibration date	Next current location
UVS-E-T 15-0124	Bentham	07-10/2019	05/2021	Saint-Denis
UVS-E-T 16-0159	Manufacturer	12/2016	06/2021	Antananarivo
UVS-E-T 16-0158	Manufacturer	06/2017	06/2021	Anse Quitor
UVS-E-T 17-0207	Manufacturer	11/2017	06/2021	Mahé
SUV-E 18-0020	Bentham	11/2019	03/2022	Maido
SUV-E 18-0028	Bentham	07/2019	03/2022	Diego Suarez
SUV-E 18-0030	Bentham	06/2019	03/2022	Fort Dauphin
SUV-E 18-0027	Bentham	08/2019	03/2022	Moroni
SUV-E 18-0029	Bentham	06/2019	03/2022	Juan de Nova

parameterisation of Allaart et al. (2004), a first estimate of UVI is computed with the TOC. The final UVI under clear sky at local solar noon (called UVI-TEMIS hereafter) is obtained by correcting the first estimates for the effects of the Earth–Sun distances, surface albedo, elevation, and aerosols (Zempila et al., 2017). The spatial resolution is $0.5 \times 0.5°$.

4.3.2 Comparison results

Ground-based UVI measurements from the UV-Indien network were compared with satellite estimates and model UVI estimates, taking the nearest model grid point or satellite pixel for each station. Then, for each satellite or model estimate computed at this point, we looked for the closest UVI-BENTHAM or UVI-RADIO measurement. Finally, for each pair of measurements, we checked the following require-

Table 4. Mean and median absolute and relative differences between CS-UVI (clear-sky UVI) satellite/model measurements and CS-UVI-RADIO at Saint-Denis. Mean and median absolute and relative differences between ALL-SKY-UVI satellite/model measurements and ALL-SKY-UVI-RADIO at Saint-Denis are in parentheses. NDATA signifies number of data points.

Stats	UVI-CAMS	UVI-OMUVBG	UVI-TROPOMI	UVI-GOME	UVI-TEMIS	UVI-BENTHAM
MEAN-AD	0.51 ± 0.63 (1.08 ± 2.19)	0.07 ± 1.89 (0.38 ± 2.47)	-0.46 ± 0.75 (0.39 ± 1.95)	-0.43 ± 1.10 (1.09 ± 2.92)	0.29 ± 0.58 (2.39 ± 3.24)	0.02 ± 0.22 (-0.02 ± 0.64)
MEAN-RD	20.12 ± 18.11 (51.13 ± 140.84)	6.22 ± 41.58 (21.24 ± 77.44)	-6.45 ± 10.87 (46.13 ± 290.98)	-3.53 ± 9.84 (34.69 ± 112.84)	1.80 ± 6.12 (57.14 ± 141.93)	4.17 ± 13.00 (1.97 ± 24.99)
MEDIAN-AD	0.21 (0.45)	−0.25 (−0.07)	−0.40 (0.02)	−0.29 (0.27)	0.20 (1.12)	0.03 (0.00)
MEDIAN-RD	15.80 (18.01)	−3.03 (−1.19)	−6.24 (0.21)	−3.08 (3.01)	2.22 (9.86)	1.45 (0.14)
NDATA	1279 (4087)	160 (467)	387 (1988)	141 (893)	164 (1069)	29 488 (92 864)

ments: the time difference between the estimate and the reference had to be less than 5 min, and the SZA difference had to be less than 5°. For these comparisons, the UVI-BENTHAM was also scaled up and linearly interpolated at a resolution of 5 min. For data from the OMUVBG and TROPOMI product, UVI estimates located within 10 km of the corresponding ground-based station were selected. For CAMS, the closest grid point available for each station was taken: 14.8, 9.6, 7.2, and 4.7 km from Antananarivo, Anse Quitor, Mahé, and Saint-Denis, respectively. For TEMIS, the closest grid point available for each station was used: 7.8, 13.0, 12.1, and 11.8 km from Antananarivo, Anse Quitor, Mahé, and Saint-Denis, respectively. Here, it was chosen to compare the satellite product or model forecast with results from the four stations of the UV-Indien network that have the longest time periods covered (Antananarivo, Anse Quitor, Mahé, and Saint-Denis). Figure 2 shows the period covered by each dataset at these four stations. Bentham has been collecting data since 2009, but, in this study, only the period between 2016 and the present was chosen because the radiometers were installed only in 2016 or later (in 2017) depending on the stations.

The Pearson correlation coefficient and absolute and relative differences were calculated for each ground-based instrument installed at each station. Then, the means and medians of the absolute and relative differences between ground-based measurements and the satellite or model estimates were computed (called Mean-AD, Median-AD, Mean-RD, and Median-RD hereafter). The correlation between the UVI-RADIO at Saint-Denis and the other measurements is shown in Fig. 3. All datasets are well correlated with the UVI-BENTHAM under clear-sky conditions; Pearson correlation coefficients are greater than 0.9 except for OMUVBG (0.55) at Saint-Denis. Correlation results for the radiometers at Saint-Denis, Antananarivo, Mahé, and Anse Quitor stations are available in the appendix (Figs. A1, A3, A5, and A7, respectively). Correlation coefficients are greater than 0.8 at all stations except Anse Quitor (for TEMIS and OMUVBG), Mahé (for OMUVBG, GOME, and TEMIS), and Saint-Denis (OMUVBG). On average, for all stations combined, OMUVBG is the product with the lowest correlation coefficients, while CAMS shows the highest correlation coefficients. Mahé is the station that is least well represented by most models, with correlation coefficients between 0.19 and 0.9.

The absolute and relative differences between satellite product or forecast model and UVI-RADIO at Saint-Denis are shown in Fig. 4 and Table 4. The clear-sky conditions are presented in blue on the boxplot (Fig. 4), and the corresponding values are reported in Table 4. The all-sky conditions are presented in red on the boxplot (Fig. 4), and the corresponding values are shown in brackets in Table 4. Looking at the median of the absolute differences (Median-AD) under all-sky conditions, it can be seen that all datasets, with the exception of OMUVBG, overestimate UVI relative to the UVI-RADIO measurements; median overestimation ranges between 0.02 (TROPOMI) and 1.12 (TEMIS). In clear-sky conditions, the median absolute differences decrease, but a UVI overestimation can still be observed for CAMS (+0.21) and TEMIS (+0.20). The smallest median difference is obtained for GOME (−0.01). UVI-RADIO is expected to be aligned with UVI-BENTHAM since it has been recalibrated with the UVI-BENTHAM measurements, so it will not be discussed here. The mean of the absolute differences under all-sky conditions ranges from 0.38 ± 2.47 (OMUVBG) to $+2.39 \pm 3.24$ (TEMIS). Under clear-sky conditions, this absolute difference is smaller and ranges between -0.46 ± 0.75 (TROPOMI) and 0.51 ± 0.63 (CAMS). The Mean-RD under all-sky conditions is between 21.24 ± 77.44 % (OMUVBG) and $+57.14 \pm 141.93$ % (TEMIS). These means and standard deviations are strongly reduced under clear-sky conditions; they are between -6.45 ± 10.87 % (GOME) and 20.12 ± 18.11 (CAMS). Similarly, the Median-RD under all-

sky conditions are higher than those obtained under clear-sky conditions. UVI estimates by satellite or models are closer to instrument measurements made on the ground in clear-sky conditions. This is mainly due to the spatial resolution and representation of clouds. The satellite pixel or model grid point is representative of a 5.6×3.7 km region for the best-defined satellite (TROPOMI) or a $0.5° \times 0.5°$ region (55 km × 55 km) (GOME, OMI, and TEMIS). Thus the cloud cover considered is representative of this entire region, but it is not necessarily that directly observed above the ground-based instruments. In addition, the pixels and grid points selected are not perfectly centred on the ground instruments. Finally, the four study sites are located in the tropics, present non-uniform topographic conditions, and are very close to the sea (with the exception of Antananarivo). These conditions favour the rapid development of clouds and complicate the estimation of cloud cover over the site by the satellite (Lakkala et al., 2020). Thus, the clear-sky conditions observed on the ground may not be the same as those observed by satellites or models. This will induce a discrepancy between UVI derived from satellites and modelling and UVI observed at the ground. For the other stations, all satellites and models underestimate the surface UVI (UVI-RADIO) except CAMS at Antananarivo, where UVI-CAMS is just above UVI-RADIO with a mean absolute difference of +0.1. The detailed results are available in the figures and tables provided in the Appendix (Figs. A1–A8 and Tables A1–A4).

Although TROPOMI has large relative differences, especially in Mahé, it is also the product with the most consistent differences. Its relative and absolute standard deviation is the smallest at all stations. It should be noted that all satellite or model estimates give poor results at the Mahé station. An examination of the percentage of clear days shows that, in Mahé, Anse Quitor, and Antananarivo, there are only 16 % clear days, while, in Saint-Denis, there are 27 % clear days. In addition, Anse Quitor and Antananarivo radiometers have a 1 min resolution, while those in Mahé and Saint-Denis have a 5 min resolution. The small number of clear-sky days combined with the larger temporal resolution reduces the number of points compared in clear-sky conditions at Mahé. Mahé station is also closer to the Equator than the other stations (at about 4° S) and is strongly influenced by the convection in this region. Outliers and large differences could be due to numerous issues. The satellite measurements and the modelled UVI do not have spatial resolutions that can accurately represent the sky conditions just above the ground-based instruments. The satellite or model grid points used in this study are either the closest grid point to the station or the average of four grid points encircling the station location. Nonetheless, for satellite estimates or model results, spatial resolution can be as large as 50 km (TEMIS or GOME) or as low as 3.7 km (TROPOMI). Also, cloud conditions, albedo, or altitude can vary strongly over distances smaller than 100 km. These differences can affect the quality of the model forecast or of the inversion algorithm used by the satellite. Differences between a satellite product or model forecast and radiometer measurements could also be explained by a drift in the radiometer calibration. Note that the radiometers installed in Mahé, Anse Quitor, and Antananarivo are still under the manufacturer's calibration, and this could explain some of the observed differences between satellite and model estimates. The recalibration of radiometers in Antananarivo, Anse Quitor, and Mahé is planned for 2021. Nevertheless, UVI-BENTHAM, which provides high-quality data and is recalibrated every 3 months, still shows a Median-RD between −2.5 % (TROPOMI) and 11.3 % (CAMS) and a Median-AD between −0.2 (TROPOMI) and 0.3 (TEMIS) in clear-sky conditions.

5 Data availability

Data from the UV radiometers and the total sky imagers can be downloaded from Zenodo and are referenced at https://doi.org/10.5281/zenodo.4811488 (Lamy and Portafaix, 2021a).

The data from the UV radiometers are also available on the WOUDC website at these addresses for the four stations studied here:

- Saint-Denis, La Réunion: https://woudc.org/data/stations/?id=530 (last access: 19 August 2021, Lamy and Portafaix, 2021b)
- Mahé, Seychelles: https://woudc.org/data/stations/?id=207 (last access: 19 August 2021, Lamy and Portafaix, 2021c)
- Anse Quitor, Mauritius: https://woudc.org/data/stations/?id=532 (last access: 19 August 2021, Lamy and Portafaix, 2021d)
- Antananarivo, Madagascar: https://woudc.org/data/stations/?id=531 (last access: 19 August 2021, Lamy and Portafaix, 2021e)

The TROPOMI surface UV radiation product used in this study is available at https://nsdc.fmi.fi/data/data_s5puv.php (last access: 1 June 2021, Lindfors et al., 2018).
The AC SAF (GOME/MetOp) data can be downloaded through the website at https://acsaf.org (last access: 1 June 2021, Kujanpää, 2021).
The TEMIS data can be downloaded through the website at http://www.temis.nl/uvradiation/UVindex.html (last access: 1 June 2021, Van Geffen et al., 2021).
The OMUVBG data can be downloaded through the website at https://disc.gsfc.nasa.gov/datasets/OMUVBG_003 (last access: 19 August 2021, Hovila et al., 2021).
The CAMS data can be downloaded through the website at https://apps.ecmwf.int (last access: 1 June 2021, Pitkänen et al., 2021).

6 Conclusions

The UV-Indien network is an emerging network dedicated to UV radiation and cloud cover in the western Indian Ocean region. This network offers numerous perspectives for studies both on the variability in these parameters at each site and, for example, for the validation of climate models. The diversity of the instrumented sites provides a good representation of the different environmental conditions in the region. Our region is essentially made up of poor countries whose access is difficult. The challenge of maintaining such a network in this region is mainly related to the regular calibration of the radiometers and also to the repair of the instruments when failures occur. A protocol including three types of calibration was established to guarantee the quality of the measurements while meeting logistical and financial constraints. A calibration plan has been established with frequencies of the order of 2 years, but logistical difficulties or health crises can modulate these forecasts. Another difficulty lies in the regular transfer of data to a centralising organisation. Nonetheless, the calibration protocol and post-processing of the data ensure the quality of the data before distribution to the Zenodo and WOUDC data repositories. In order to assess the validity of the measurements so that future users can use them with confidence, we compared these measurements with satellite estimates and model estimates of the UVI. In clear-sky conditions, the correlation coefficient between the satellite or model estimates and the ground-based measurements was greater than 0.9 at all stations except Mahé and for all datasets except OMUVBG. In all-sky conditions, the largest UVI median absolute difference between the satellite or model estimates and the ground-based instruments was −0.4 (TROPOMI), −1.4 (TROPOMI), −2.3 (GOME), and −6.0 (GOME) at Saint-Denis, Antananarivo, Anse Quitor, and Mahé, respectively. In clear-sky conditions, the largest UVI median absolute difference between the satellites or model estimates and the ground-based instruments was 1.1 (TEMIS), −1.3 (TROPOMI), −1.7 (GOME), and −4.6 (GOME) at Saint-Denis, Antananarivo, Anse Quitor, and Mahé, respectively. In all-sky conditions, the smallest UVI median difference between the satellites or model estimates and the measurements of ground-based instruments was 0.1 (CAMS and TEMIS), −0.1 (CAMS), −0.1 (CAMS), and 0.1 (CAMS) at Saint-Denis, Antananarivo, Anse Quitor, and Mahé, respectively. In clear-sky conditions, the smallest UVI median difference between the satellites or model estimates and the measurements of ground-based instruments was 0.02 (TROPOMI), 0.04 (OMUVBG), −0.1 (CAMS), and −0.4 (CAMS) at Saint-Denis, Antananarivo, Anse Quitor, and Mahé, respectively. Compared to ground measurements, UVI-CAMS showed the most consistent results at all stations in both all-sky and clear-sky conditions. At Saint-Denis, satellite and model estimates were usually found to overestimate UVI compared to ground-based instruments, while at Antananarivo, Anse Quitor, and Mahé, satellite and model estimates were found to underestimate ground-based measurements of UVI.

The largest discrepancies were observed at the Mahé station. Many reasons can be evoked to explain these differences. The satellite or model resolution may not be able to accurately determine the sky conditions above the station. As Mahé is under the influence of the sea breeze, the formation of clouds is frequent late in the morning. From the ground, these clouds could be seen to induce irradiance enhancements due to multiple scattering at their edges. From the satellite's point of view, only strong backscattering would be observed, and an attenuation of the clouds would therefore be applied to the UV product. This is also consistent with the time of the satellite estimates (solar noon or overpass), which is late in the morning when cloud formation is frequent which would induce backscattering. UVI enhancement also occurs frequently during this time (Fig. 5). These two phenomena could explain both the observed high UVI and the discrepancy with satellite and model estimates. A drift in the radiometer calibration could also explain part of the difference. In addition, Mahé presents a small number of clear-sky comparison points since the Kipp and Zonen radiometer temporal resolution is 5 min and there are only 16 % clear-sky days. Saint-Denis and Anse Quitor are mountainous islands also under the influence of trade winds, where there is frequent cloud formation in the late morning. A fractional cloud sky cover could induce UVI enhancements measured by the ground-based instruments, while satellites and models could apply attenuation of the measured UVI instead. These two stations are located at about 20° S, while Mahé is located at about 5° S. Therefore, the maxima of UVI are higher at Mahé, and the resulting enhancement of UVI should also be stronger. As the phenomenon of cloud enhancement of the UV index can be observed in the radiometer data of the four stations presented in detail here, these data are suitable for the study of this phenomenon. To enable users to investigate the impact of clouds on UVI, all-sky cameras have recently been deployed at each station of the UV-Indien network. In this article, we have also proposed a first estimate of the variability in UVI at these different sites to give users a general idea of this variability. In a region where UVI values are very high all year round, these data are also useful for monitoring the intensity of ultraviolet radiation in the Indian Ocean for preventive health studies or health impact studies. The monitoring of long-term UVI trends in the region will allow us to evaluate their evolution in the context of climate change and the possible acceleration of the Brewer–Dobson circulation leading to a decrease in the total ozone column in the tropics and thus an increase in ultraviolet radiation levels.

Appendix A

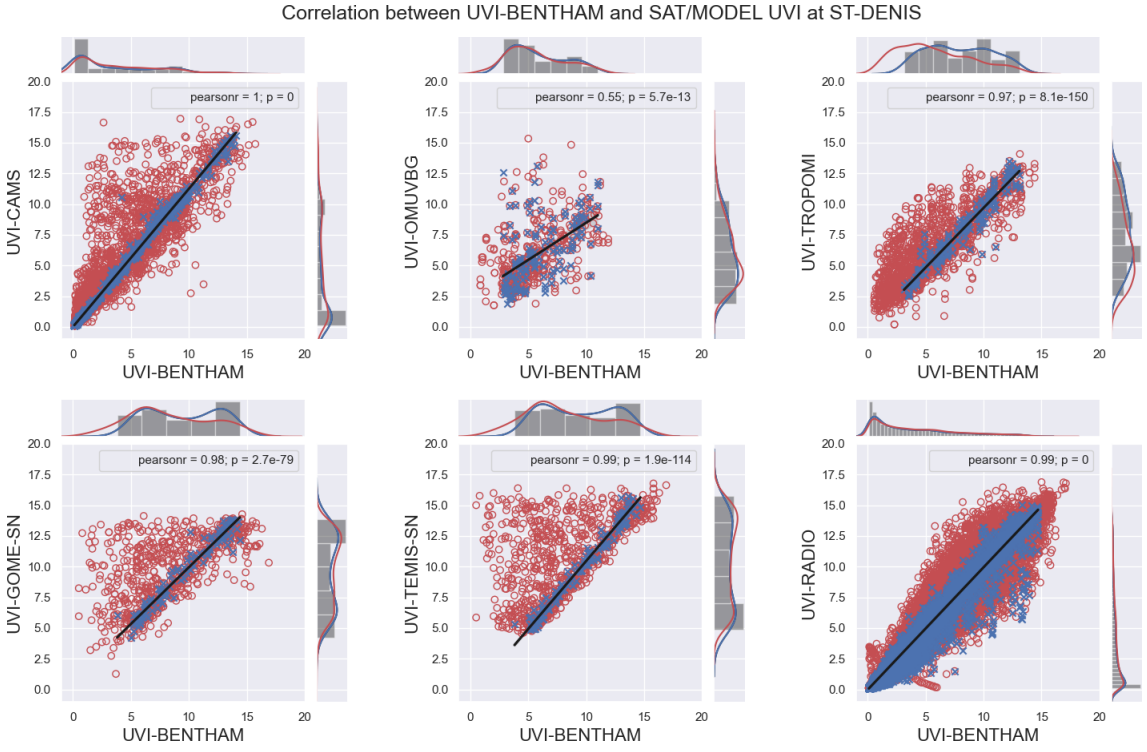

Figure A1. Correlation between UVI-BENTHAM and satellite/model estimates at Saint-Denis. A histogram representing each dataset distribution is represented at the right and at the top side of each subfigure. The clear-sky measurements made by UVI-RADIO have been distinguished and are shown as blue crosses, while the measurements for all-sky conditions are shown as red circles.

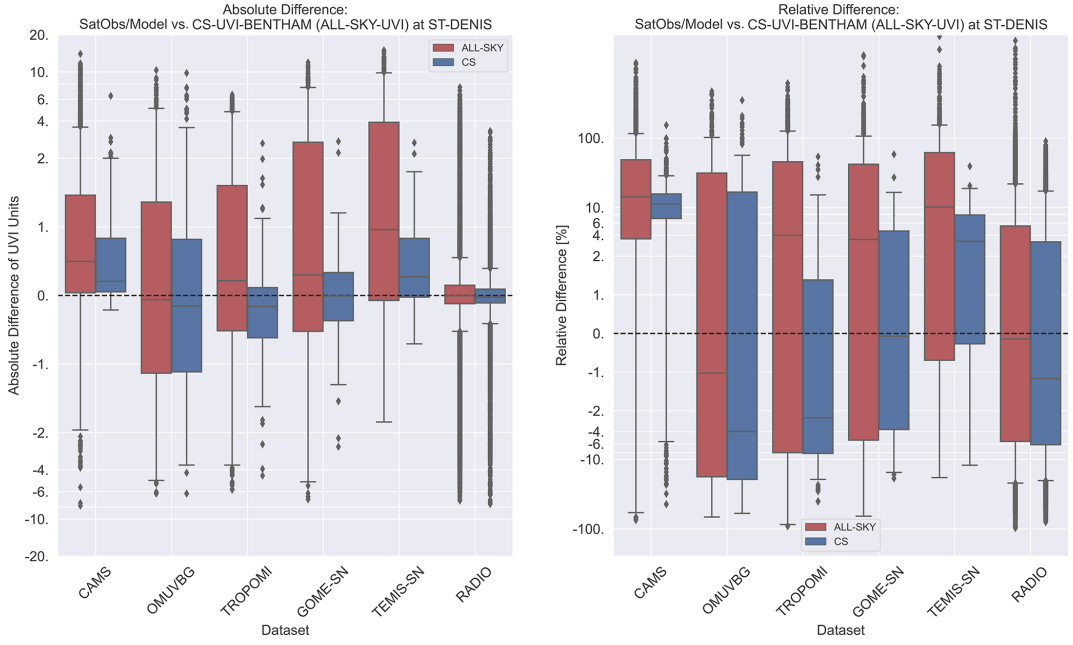

Figure A2. Boxplot of differences between UVI-RADIO and satellite/model estimates at Saint-Denis.

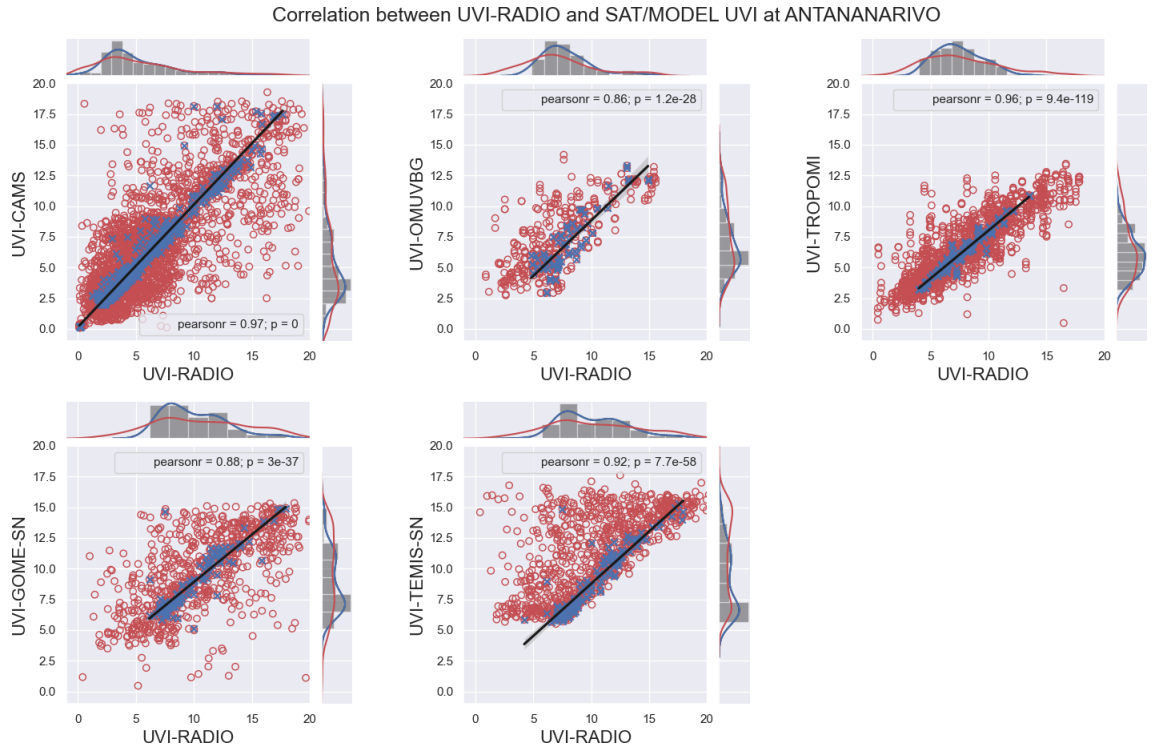

Figure A3. Correlation between UVI-RADIO and satellite/model estimates at Antananarivo. A histogram representing each dataset distribution is represented at the right and at the top side of each subfigure. The clear-sky measurements made by UVI-RADIO have been distinguished and are shown as blue crosses, while the measurements for all-sky conditions are shown as red circles.

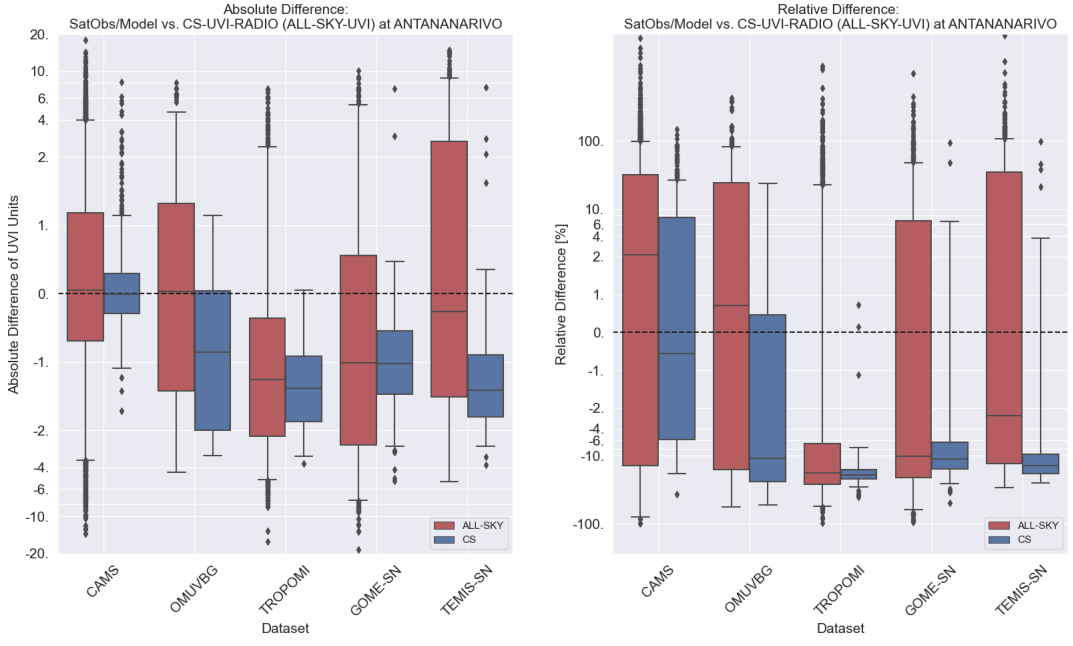

Figure A4. Boxplot of differences between UVI-RADIO and satellite/model estimates at Antananarivo.

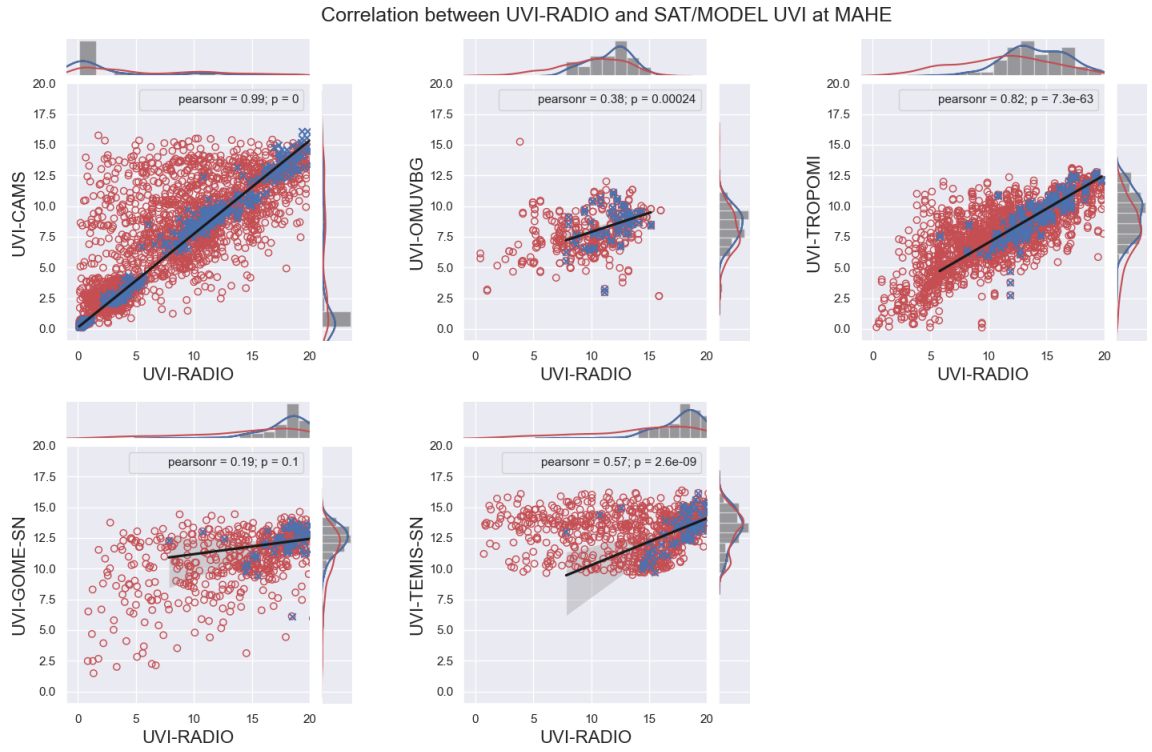

Figure A5. Correlation between UVI-RADIO and satellite/model estimates at Mahé. A histogram representing each dataset distribution is represented at the right and at the top side of each subfigure. The clear-sky measurements made by UVI-RADIO have been distinguished and are shown as blue crosses, while the measurements for all-sky conditions are shown as red circles.

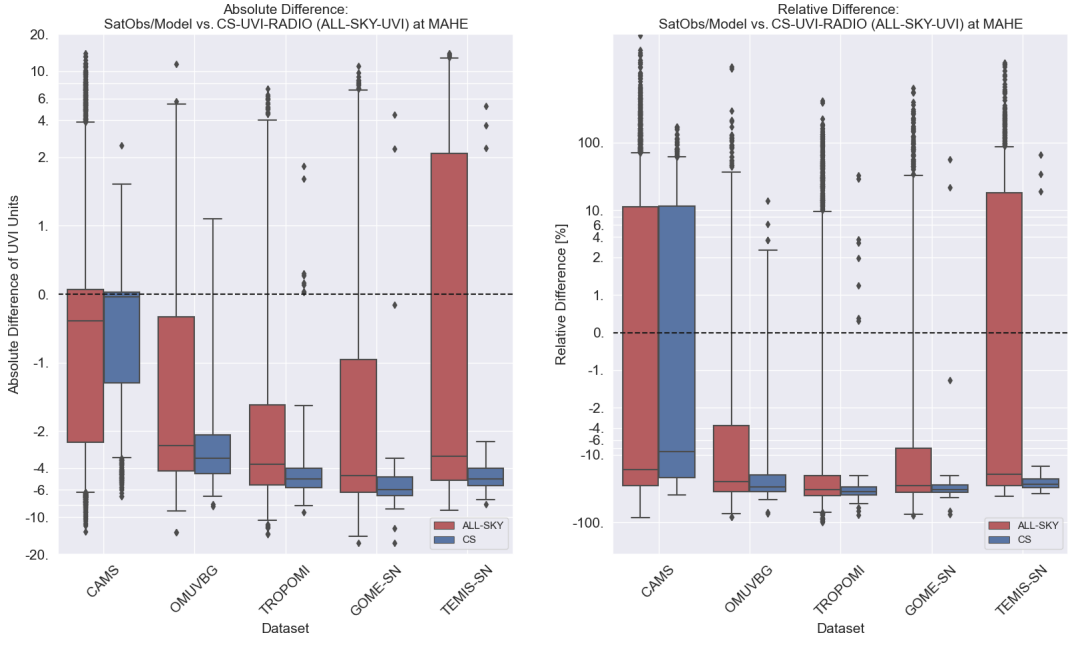

Figure A6. Boxplot of differences between UVI-RADIO and satellite/model estimates at Mahé.

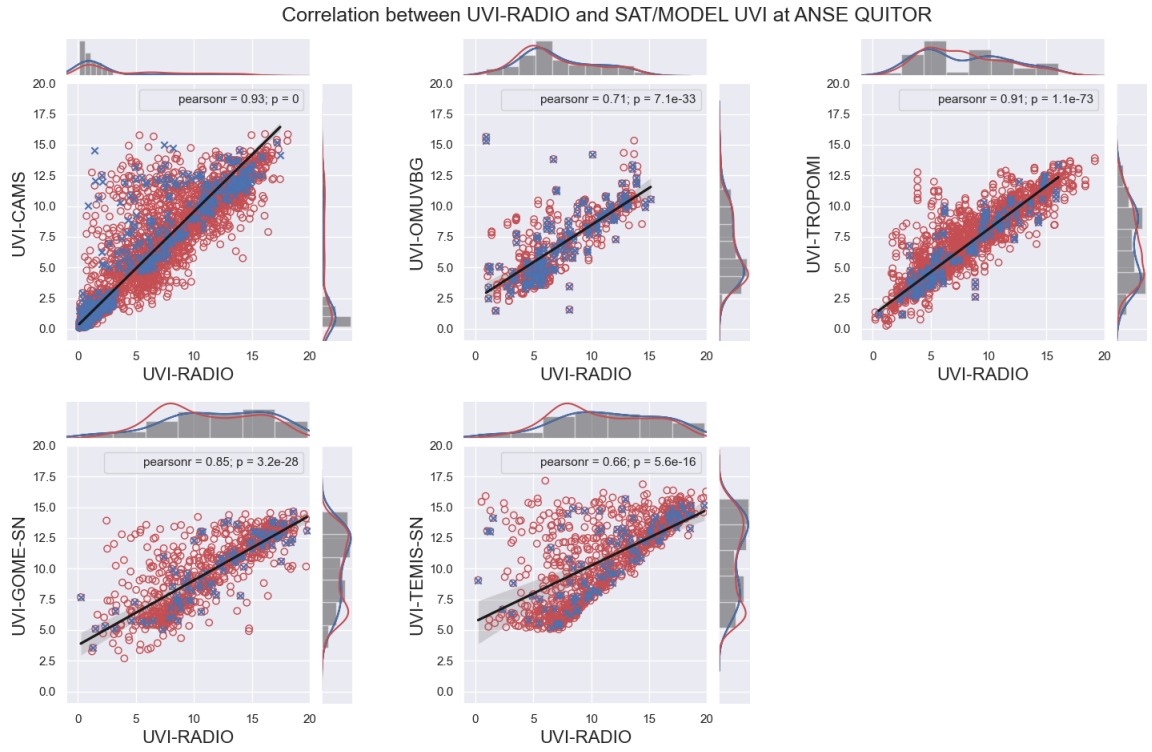

Figure A7. Correlation between UVI-RADIO and satellite/model estimates at Anse Quitor. A histogram representing each dataset distribution is represented at the right and at the top side of each subfigure. The clear-sky measurements made by UVI-RADIO have been distinguished and are shown as blue crosses, while the measurements for all-sky conditions are shown as red circles.

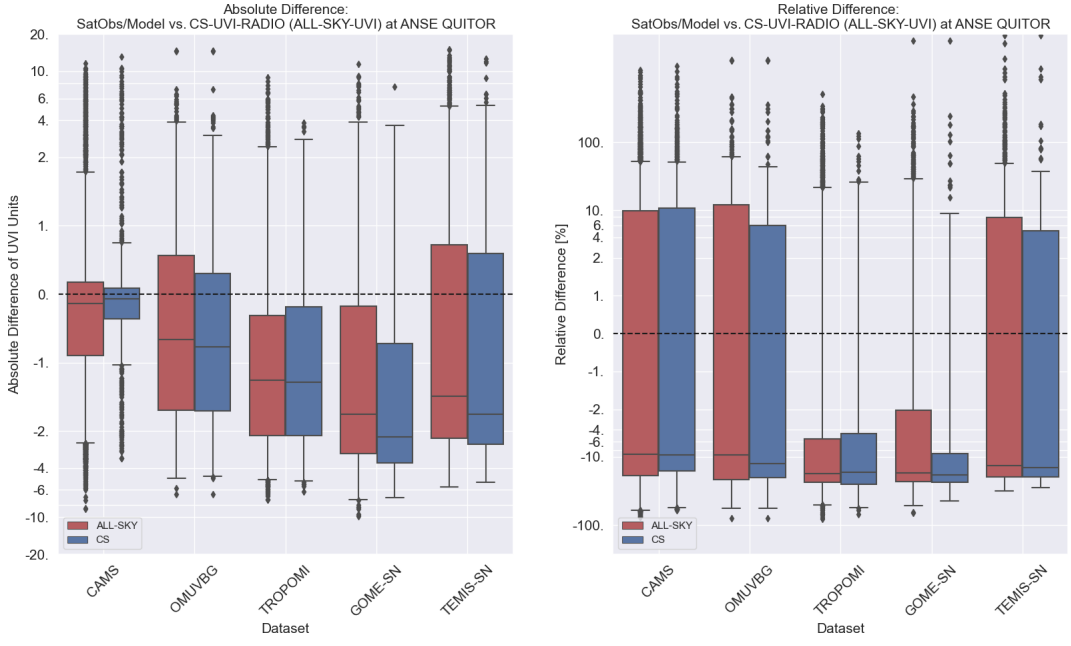

Figure A8. Boxplot of differences between UVI-RADIO and satellite/model estimates at Anse Quitor.

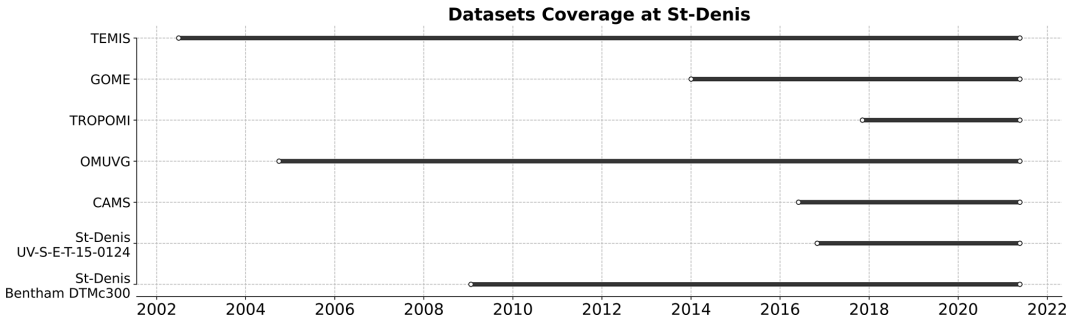

Figure A9. Timeline of the instruments of the UVI dataset used in the comparison at Saint-Denis.

Table A1. Mean and median absolute and relative differences between CS-UVI satellite/model measurements and CS-UVI-BENTHAM at Saint-Denis. Mean and median absolute and relative differences between ALL-SKY-UVI satellite/model measurements and ALL-SKY-UVI-BENTHAM at Saint-Denis are in parentheses.

Stats	UVI-CAMS	UVI-OMUVBG	UVI-TROPOMI	UVI-GOME	UVI-TEMIS	UVI-RADIO
MEAN-AD	0.47 ± 0.55 (1.09 ± 1.97)	0.09 ± 2.36 (0.34 ± 2.54)	-0.25 ± 0.73 (0.60 ± 1.83)	-0.01 ± 0.68 (1.23 ± 2.86)	0.40 ± 0.62 (2.31 ± 3.26)	-0.03 ± 0.39 (0.02 ± 0.65)
MEAN-RD	12.33 ± 12.27 (48.36 ± 105.87)	8.54 ± 53.93 (23.95 ± 82.00)	-3.13 ± 10.09 (30.85 ± 70.85)	0.78 ± 8.66 (40.31 ± 123.55)	3.61 ± 7.12 (59.73 ± 164.38)	-2.95 ± 12.16 (0.32 ± 23.77)
MEDIAN-AD	0.21 (0.50)	−0.15 (−0.06)	−0.16 (0.21)	−0.01 (0.30)	0.27 (0.96)	−0.02 (−0.00)
MEDIAN-RD	11.32 (14.20)	−3.98 (−1.03)	−2.52 (3.98)	−0.07 (3.48)	3.27 (10.15)	−1.17 (−0.14)
NDATA	1038 (3069)	145 (408)	254 (1555)	120 (750)	142 (919)	34 665 (93 300)

Table A2. Mean and median absolute and relative differences between CS-UVI satellite/model measurements and CS-UVI-RADIO at Antananarivo. Mean and median absolute and relative differences between ALL-SKY-UVI satellite/model measurements and ALL-SKY-UVI-RADIO at Antananarivo are in parentheses.

Stats	UVI-CAMS	UVI-OMUVBG	UVI-TROPOMI	UVI-GOME	UVI-TEMIS
MEAN-AD	0.14 ± 0.84 (0.18 ± 2.64)	-0.96 ± 1.16 (0.10 ± 2.24)	-1.43 ± 0.61 (-1.35 ± 1.91)	-1.10 ± 1.27 (-1.00 ± 3.23)	-1.25 ± 1.11 (0.77 ± 3.20)
MEAN-RD	4.03 ± 18.53 (21.40 ± 113.35)	-12.16 ± 15.84 (13.53 ± 58.09)	-18.94 ± 5.65 (-8.93 ± 61.87)	-10.09 ± 13.80 (1.39 ± 58.78)	-11.96 ± 13.22 (26.44 ± 139.83)
MEDIAN-AD	−0.01 (0.05)	−0.86 (0.04)	−1.38 (−1.26)	−1.02 (−1.01)	−1.41 (−0.26)
MEDIAN-RD	−0.55 (2.13)	−10.98 (0.71)	−19.11 (−18.02)	−11.11 (−10.10)	−14.13 (−2.59)
NDATA	564 (3337)	92 (427)	203 (1796)	111 (816)	142 (992)

Table A3. Mean and median absolute and relative differences between CS-UVI satellite/model measurements and CS-UVI-RADIO at Mahé. Mean and median absolute and relative differences between ALL-SKY-UVI satellite/model measurements and ALL-SKY-UVI-RADIO at Mahé are in parentheses.

Stats	UVI-CAMS	UVI-OMUVBG	UVI-TROPOMI	UVI-GOME	UVI-TEMIS
MEAN-AD	-0.82 ± 1.44 (-0.93 ± 2.94)	-3.22 ± 1.83 (-2.16 ± 2.95)	-4.80 ± 1.60 (-3.48 ± 2.88)	-5.75 ± 2.51 (-3.41 ± 4.29)	-4.52 ± 1.82 (-1.22 ± 4.99)
MEAN-RD	-1.23 ± 28.57 (11.52 ± 140.58)	-26.62 ± 14.30 (-6.28 ± 101.10)	-33.43 ± 10.43 (-24.98 ± 31.94)	-30.65 ± 14.98 (-6.92 ± 69.82)	-24.46 ± 13.08 (23.62 ± 144.59)
MEDIAN-AD	-0.04 (-0.39)	-3.31 (-2.63)	-4.88 (-3.73)	-5.99 (-4.59)	-4.91 (-3.19)
MEDIAN-RD	-8.91 (-16.41)	-29.49 (-24.85)	-34.58 (-32.70)	-32.25 (-28.55)	-27.11 (-19.15)
NDATA	1133 (3525)	89 (392)	253 (2132)	72 (635)	94 (881)

Table A4. Mean and median absolute and relative differences between CS-UVI satellite/model measurements and CS-UVI-RADIO at Anse Quitor. Mean and median absolute and relative differences between ALL-SKY-UVI satellite/model measurements and ALL-SKY-UVI-RADIO at Anse Quitor are in parentheses.

Stats	UVI-CAMS	UVI-OMUVBG	UVI-TROPOMI	UVI-GOME	UVI-TEMIS
MEAN-AD	0.06 ± 1.49 (-0.20 ± 1.82)	-0.43 ± 2.36 (-0.36 ± 2.19)	-1.28 ± 1.69 (-1.19 ± 1.80)	-1.88 ± 2.58 (-1.42 ± 2.71)	-0.55 ± 3.34 (-0.39 ± 3.06)
MEAN-RD	12.02 ± 91.52 (6.85 ± 69.67)	17.36 ± 163.36 (12.16 ± 114.22)	-10.93 ± 26.62 (-8.71 ± 35.26)	26.16 ± 319.83 (0.12 ± 121.81)	56.15 ± 376.30 $18.21 \pm 179.43)$
MEDIAN-AD	-0.06 (-0.14)	-0.77 (-0.66)	-1.28 (-1.25)	-2.23 (-1.75)	-1.75 (-1.49)
MEDIAN-RD	-9.28 (-9.20)	-12.56 (-9.45)	-16.65 (-17.68)	-18.47 (-17.10)	-14.51 (-13.31)
NDATA	996 (3956)	204 (516)	189 (2114)	95 (752)	115 (964)

Author contributions. KeL and TP wrote the original draft. CB, KaL, AA, and MAT reviewed the manuscript. MRAP developed and validated the CAMS data. JBP was the technical manager of the UV-Indien Network. VA is the technical manager of Mahé Station. MAT is the technical manager of Moroni Station. SR is the technical manager of Antananarivo Station.

Competing interests. The authors declare that they have no conflict of interest.

Disclaimer. Publisher's note: Copernicus Publications remains neutral with regard to jurisdictional claims in published maps and institutional affiliations.

Acknowledgements. We thank the AC SAF project of EUMETSAT for providing the GOME-2/MetOp offline surface UV products used in this paper. We also thank the Finnish Meteorological Institute for providing the TROPOMI UV products and especially Jukka Kujanpää for product development. The authors thank Reuniwatt for the support provided during the installation of the total sky cameras at the different sites of the UV-Indien network. Finally, the authors would like to thank the PMOD/WRC for carrying out the calibration of the UVS-E-T-150154 radiometer in Moufia, Saint-Denis.

Financial support. The UV-Indien programme is supported by the European Union through PO INTERREG V, by the Reunion Island Council, and by the French Government. The Bentham spectroradiometer and UV radiometer at Saint-Denis are managed by OPAR (Observatoire de Physique de l'Atmosphère de la Réunion), and OPAR activities are funded by the Université de La Réunion and CNRS. Measurements of Bentham spectroradiometers are also supported by CNES (within the French programme TOSCA).

Review statement. This paper was edited by Nellie Elguindi and reviewed by two anonymous referees.

References

Arola, A., Kazadzis, S., Lindfors, A., Krotkov, N., Kujanpää, J., Tamminen, J., Bais, A., di Sarra, A., Villaplana, J. M., Brogniez, C., Siani, A. M., Janouch, M., Weihs, P., Webb, A., Koskela, T., Kouremeti, N., Meloni, D., Buchard, V., Auriol, F., Ialongo, I., Staneck, M., Simic, S., Smedley, A., and Kinne, S.: A new approach to correct for absorbing aerosols in OMI UV, Geophys. Res. Lett., 36, L22805, https://doi.org/10.1029/2009GL041137, 2009.

Badosa, J., Calbó, J., Mckenzie, R., Liley, B., González, J.-A., Forgan, B., and Long, C. N.: Two Methods for Retrieving UV Index for All Cloud Conditions from Sky Imager Products or Total SW Radiation Measurements, Photochemistry and Photobiology, 90, 941–951, https://doi.org/10.1111/php.12272, 2014.

Baray, J.-L., Courcoux, Y., Keckhut, P., Portafaix, T., Tulet, P., Cammas, J.-P., Hauchecorne, A., Godin Beekmann, S., De Mazière, M., Hermans, C., Desmet, F., Sellegri, K., Colomb, A., Ramonet, M., Sciare, J., Vuillemin, C., Hoareau, C., Dionisi, D., Duflot, V., Vérèmes, H., Porteneuve, J., Gabarrot, F., Gaudo, T., Metzger, J.-M., Payen, G., Leclair de Bellevue, J., Barthe, C., Posny, F., Ricaud, P., Abchiche, A., and Delmas, R.: Maïdo observatory: a new high-altitude station facility at Reunion Island (21° S, 55° E) for long-term atmospheric remote sensing and in situ measurements, Atmos. Meas. Tech., 6, 2865–2877, https://doi.org/10.5194/amt-6-2865-2013, 2013.

Bernhard, G. H., Neale, R. E., Barnes, P. W., Neale, P., Zepp, R. G., Wilson, S. R., Andrady, A. L., Bais, A. F., McKenzie, R., Aucamp, P. J., Young, P. J., Liley, J. B., Lucas, R. M., Yazar, S., Rhodes, L. E., Byrne, S. N., Hollestein, L. M., Olsen, C. M., Young, A. R., Robson, T. M., Bornman, J. F., Jansen, M. A. K., Robinson, S. A., Ballaré, C. L., Williamson, C. E., Rose, K. C., Banaszak, A. T., Häder, D.-P., Hylander, S., Wängberg, S., Austin, A. T., Hou, W.-C., Paul, N. D., Madronich, S., Sulzberger, B., Solomon, K. R., Li, H., Schikowski, T., Longstreth, J., Pandey, K. K., Heikkilä, A. M., and White, C. C.: Environmental effects of stratospheric ozone depletion, UV radiation and interactions with climate change: UNEP Environmental Effects Assessment Panel, update 2019, Photochemical & Photobiological Sciences, 19, 542–584, 2020.

Bouillon, R., Eisman, J., Garabedian, M., Holick, M., Kleinschmidt, J., Suda, T., Terenetskaya, I., and Webb, A.: Action Spectrum for the Production of Pre-vitamin D3 in Human Skin: CIE 174-2006, International Commission on Illumination, Wien, Austria, 2006.

Bozzo, A., Arola A., Cesnulyte, V., and Pitkänen, M.: Report on implementation of spectral UV irradiance, MACC-III deliverable D57.2, work package 122, Tech. rep., 2015.

Brogniez, C., Auriol, F., Deroo, C., Arola, A., Kujanpää, J., Sauvage, B., Kalakoski, N., Pitkänen, M. R. A., Catalfamo, M., Metzger, J.-M., Tournois, G., and Da Conceicao, P.: Validation of satellite-based noontime UVI with NDACC ground-based instruments: influence of topography, environment and satellite overpass time, Atmos. Chem. Phys., 16, 15049–15074, https://doi.org/10.5194/acp-16-15049-2016, 2016.

Butchart, N.: The Brewer-Dobson circulation, Rev. Geophys., 52, 157–184, https://doi.org/10.1002/2013rg000448, 2014.

Butler, A. H., Daniel, J. S., Portmann, R. W., Ravishankara, A. R., Young, P. J., Fahey, D. W., and Rosenlof, K. H.: Diverse policy implications for future ozone and surface UV in a changing climate, Environ. Res. Lety., 11, 064017, https://doi.org/10.1088/1748-9326/11/6/064017, 2016.

Cadet, J.-M., Portafaix, T., Bencherif, H., Lamy, K., Brogniez, C., Auriol, F., Metzger, J.-M., Boudreault, L.-E., and Wright, C. Y.: Inter-Comparison Campaign of Solar UVR Instruments under Clear Sky Conditions at Reunion Island (21° S, 55° E), Int. J. Environ. Res. Public Health, 17, 2867, https://doi.org/10.3390/ijerph17082867, 2020.

Calbó, J., Pagès, D., and González, J.-A.: Empirical studies of cloud effects on UV radiation: A review, Rev. Geophys., 43, RG2002, https://doi.org/10.1029/2004RG000155, 2005.

Chipperfield, M. P., Dhomse, S. S., Feng, W., McKenzie, R., Velders, G. J., and Pyle, J. A.: Quantifying the ozone and ultraviolet benefits already achieved by the Montreal Protocol, Nat. Commun., 6, 7233, https://doi.org/10.1038/ncomms8233, 2015.

CIE Standard: Erythema reference action spectrum and standard erythema dose, CIE S 007, E1998, 1998.

Duan, S.-M., Zhao, X.-S., Wen, R.-F., Huang, J.-J., Pi, G.-H., Zhang, S.-X., Han, J., Bi, S.-L., Ruan, L., Dong, X.-P., and SARS Research Team: Stability of SARS coronavirus in human specimens and environment and its sensitivity to heating and UV irradiation, Biomed. Environ. Sci., 16, 246—255, 2003.

Eyring, V., Lamarque, J.-F., Hess, P., Arfeuille, F., Bowman, K., Chipperfiel, M. P., Duncan, B., Fiore, A., Gettelman, A., Giorgetta, M. A., Granier, C., Hegglin, M., Kinnison, D., Kunze, M., Langematz, U., Luo, B., Martin, R., Matthes, K., Newman, P. A., Peter, T., Robock, A., Ryerson, T., Saiz-Lopez, A., Salawitch, R., Schultz, M., Shepherd, T. G., Shindell, D., Stähelin, J., Tegtmeier, S., Thomason, L., Tilmes, S., Vernier, J.-P., Waugh, D. W., and Young, P. J.: Overview of IGAC/SPARC Chemistry-Climate Model Initiative (CCMI) community simulations in support of upcoming ozone and climate assessments, SPARC newsletter, 40, 48–66, 2013.

Garane, K., Koukouli, M.-E., Verhoelst, T., Lerot, C., Heue, K.-P., Fioletov, V., Balis, D., Bais, A., Bazureau, A., Dehn, A., Goutail, F., Granville, J., Griffin, D., Hubert, D., Keppens, A., Lambert, J.-C., Loyola, D., McLinden, C., Pazmino, A., Pommereau, J.-P., Redondas, A., Romahn, F., Valks, P., Van Roozendael, M., Xu, J., Zehner, C., Zerefos, C., and Zimmer, W.: TROPOMI/S5P total ozone column data: global ground-based validation and consistency with other satellite missions, Atmos. Meas. Tech., 12, 5263–5287, https://doi.org/10.5194/amt-12-5263-2019, 2019.

Gorremans, M. and Masquelier, B.: Risques environnementaux et développement: Le cas de la pollution de l'air à Antananarivo, Madagascar, Faculté des sciences économiques, sociales, politiques et de communication, Université catholique de Louvain, 2018.

Herman, J. R., Labow, G., Hsu, N. C., and Larko, D.: Changes in cloud and aerosol cover (1980-2006) from reflectivity time series using SeaWiFS, N7-TOMS, EP-TOMS, SBUV-2, and OMI radiance data, J. Geophys. Res.-Atmos., 114, D01201, https://doi.org/10.1029/2007JD009508, 2009.

Holben, B., Eck, T., Slutsker, I., Tanré, D., Buis, J., Setzer, A., Vermote, E., Reagan, J., Kaufman, Y., Nakajima, T., Lavenu, F., Jankowiak, I., and Smirnov, A.: AERONET—A Federated Instrument Network and Data Archive for Aerosol Characterization, Remote Sens. Environ., 66, 1–16, https://doi.org/10.1016/S0034-4257(98)00031-5, 1998.

Hovila, J., Arola, A., and Tamminen, J.: OMI/Aura Surface UVB Irradiance and Erythemal Dose Daily L2 Global Gridded 0.25° × 0.25° V3 (OMUVBG), [data set], available at: https://disc.gsfc.nasa.gov/datasets/OMUVBG_003, last access: 19 August 2021.

Hume, J. P., Göhlich, U., and Kroh, A.: A synopsis of the prehuman avifauna of the Mascarene Islands, in: Paleornithological Research 2013: Proceedings of the 8th International Meeting of the Society of Avian Paleontology and Evolution, Vienna, Austria, 195–237, 2013.

Kabanov, D., Sakerin, S., and Turchinovich, S.: Sun photometer for scientific monitoring (instrumentation, techniques, algorithms), translated by: Terpugova, S. A., edited by: Ponomareva, S. B., Atmospheric And Oceanic Optics C/C Of Optika Atmosfery I Okeana, Springer Science and Media, 14, 1067–1074, 2001.

Kinne, S., O'Donnel, D., Stier, P., Kloster, S., Zhang, K., Schmidt, H., Rast, S., Giorgetta, M., Eck, T. F., and Stevens, B.: MAC-v1: A new global aerosol climatology for climate studies, J. Adv. Model. Earth Sy., 5, 704–740, https://doi.org/10.1002/jame.20035, 2013.

Krotkov, N. A., Bhartia, P. K., Herman, J. R., Fioletov, V., and Kerr, J.: Satellite estimation of spectral surface UV irradiance in the presence of tropospheric aerosols: 1. Cloud-free case, J. Geophys. Res.-Atmos., 103, 8779–8793, https://doi.org/10.1029/98JD00233, 1998.

Kujanpää, J.: AC SAF offline surface UV, [data set], available at: https://acsaf.org, last access: 1 June 2021.

Kujanpää, J. and Kalakoski, N.: Operational surface UV radiation product from GOME-2 and AVHRR/3 data, Atmos. Meas. Tech., 8, 4399–4414, https://doi.org/10.5194/amt-8-4399-2015, 2015.

Lakkala, K., Kujanpää, J., Brogniez, C., Henriot, N., Arola, A., Aun, M., Auriol, F., Bais, A. F., Bernhard, G., De Bock, V., Catalfamo, M., Deroo, C., Diémoz, H., Egli, L., Forestier, J.-B., Fountoulakis, I., Garane, K., Garcia, R. D., Gröbner, J., Hassinen, S., Heikkilä, A., Henderson, S., Hülsen, G., Johnsen, B., Kalakoski, N., Karanikolas, A., Karppinen, T., Lamy, K., León-Luis, S. F., Lindfors, A. V., Metzger, J.-M., Minvielle, F., Muskatel, H. B., Portafaix, T., Redondas, A., Sanchez, R., Siani, A. M., Svendby, T., and Tamminen, J.: Validation of the TROPOspheric Monitoring Instrument (TROPOMI) surface UV radiation product, Atmos. Meas. Tech., 13, 6999–7024, https://doi.org/10.5194/amt-13-6999-2020, 2020.

Lamy, K. and Portafaix, T.: Ultraviolet Index measurements in the Indian Ocean, Zenodo, https://doi.org/10.5281/zenodo.4572026, 2021a.

Lamy, K. and Portafaix, T.: UV Radiometers in the Indian Ocean, [data set], available at: https://woudc.org/data/stations/?id=530, last access: 19 August 2021b.

Lamy, K. and Portafaix, T.: UV Radiometers in the Indian Ocean, [data set], available at: https://woudc.org/data/stations/?id=207, last access: 19 August 2021b.

Lamy, K. and Portafaix, T.: UV Radiometers in the Indian Ocean, [data set], available at: https://woudc.org/data/stations/?id=532, last access: 19 August 2021d.

Lamy, K. and Portafaix, T.: UV Radiometers in the Indian Ocean, [data set], available at: https://woudc.org/data/stations/?id=531, last access: 19 August 2021e.

Lamy, K., Portafaix, T., Josse, B., Brogniez, C., Godin-Beekmann, S., Bencherif, H., Revell, L., Akiyoshi, H., Bekki, S., Hegglin, M. I., Jöckel, P., Kirner, O., Liley, B., Marecal, V., Morgenstern, O., Stenke, A., Zeng, G., Abraham, N. L., Archibald, A. T., Butchart, N., Chipperfield, M. P., Di Genova, G., Deushi, M., Dhomse, S. S., Hu, R.-M., Kinnison, D., Kotkamp, M., McKenzie, R., Michou, M., O'Connor, F. M., Oman, L. D., Pitari, G., Plummer, D. A., Pyle, J. A., Rozanov, E., Saint-Martin, D., Sudo, K., Tanaka, T. Y., Visioni, D., and Yoshida, K.: Clear-sky ultraviolet radiation modelling using output from the Chemistry Climate Model Initiative, Atmos. Chem. Phys., 19, 10087–10110, https://doi.org/10.5194/acp-19-10087-2019, 2019.

Levelt, P. F., van den Oord, G. H. J., Dobber, M. R., Malkki, A., Huib Visser, Johan de Vries, Stammes, P., Lundell, J. O. V., and Saari, H.: The ozone monitoring instrument, IEEE T. Geosci. Remote, 44, 1093–1101, https://doi.org/10.1109/TGRS.2006.872333, 2006.

Lindfors, A. V., Kujanpää, J., Kalakoski, N., Heikkilä, A., Lakkala, K., Mielonen, T., Sneep, M., Krotkov, N. A., Arola, A., and Tamminen, J.: The TROPOMI surface UV algorithm, Atmos. Meas. Tech., 11, 997–1008, https://doi.org/10.5194/amt-11-997-2018, 2018.

Lothon, M., Barnéoud, P., Gabella, O., Lohou, F., Derrien, S., Rondi, S., Chiriaco, M., Bastin, S., Dupont, J.-C., Haeffelin, M., Badosa, J., Pascal, N., and Montoux, N.: ELIFAN, an algorithm for the estimation of cloud cover from sky imagers, Atmos. Meas. Tech., 12, 5519–5534, https://doi.org/10.5194/amt-12-5519-2019, 2019.

Madronich, S.: Analytic Formula for the Clear-sky UV Index, Photochem. Photobiol. 83, 1537–1538, https://doi.org/10.1111/j.1751-1097.2007.00200.x, 2007.

Observatoire Régional de la Santé de La Réunion: Melanome Cutane à la Réunion, Technical Report, 2008.

Pastel, M., Pommereau, J.-P., Goutail, F., Richter, A., Pazmiño, A., Ionov, D., and Portafaix, T.: Construction of merged satellite total O_3 and NO_2 time series in the tropics for trend studies and evaluation by comparison to NDACC SAOZ measurements, Atmos. Meas. Tech., 7, 3337–3354, https://doi.org/10.5194/amt-7-3337-2014, 2014.

Pitkänen, M. R. A., Wandji, W., and Arola, A.: Validation Report of the CAMS UV processor, Issue #20, June-July-August(JJA) 2020: Solar radiation products, Tech. rep., ECMWF Copernicus Report, 2020.

Pitkänen, M. R. A., Wandji, W., and Arola, A.: CAMS Near-real-time, [data set], available at: https://apps.ecmwf.int last access: 1 June 2021.

Sabburg, J. and Wong, J.: The effect of clouds on enhancing UVB irradiance at the Earth's surface: A one year study, Geophys. Res. Lett., 27, 3337–3340, https://doi.org/10.1029/2000GL011683, 2000.

Sitek, A., Rosset, I., Żądzińska, E., Kasielska-Trojan, A., Neskoromna-Jędrzejczak, A., and Antoszewski, B.: Skin color parameters and Fitzpatrick phototypes in estimating the risk of skin cancer: A case-control study in the Polish population, J. Am. Acad. Dermatol., 74, 716 – 723, https://doi.org/10.1016/j.jaad.2015.10.022, 2016.

Strasberg, D., Rouget, M., Richardson, D. M., Baret, S., Dupont, J., and Cowling, R. M.: An assessment of habitat diversity and transformation on La Réunion Island (Mascarene Islands, Indian Ocean) as a basis for identifying broad-scale conservation priorities, Biodiv. Conserv., 14, 3015–3032, 2005.

Tanskanen, A., Krotkov, N. A., Herman, J. R., and Arola, A.: Surface ultraviolet irradiance from OMI, IEEE T. Geosci. Remote, 44, 1267–1271, 2006.

Tanskanen, A., Lindfors, A., Määttä, A., Krotkov, N., Herman, J., Kaurola, J., Koskela, T., Lakkala, K., Fioletov, V., Bernhard, G., McKenzie, R., Kondo, Y., O'Neill, M., Slaper, H., den Outer, P., Bais, A. F., and Tamminen, J.: Validation of daily erythemal doses from Ozone Monitoring Instrument with ground-based UV measurement data, J. Geophys. Res., 112, D24S44, https://doi.org/10.1029/2007jd008830, 2007.

Toihir, A. M., Portafaix, T., Sivakumar, V., Bencherif, H., Pazmiño, A., and Bègue, N.: Variability and trend in ozone over the southern tropics and subtropics, Ann. Geophys., 36, 381–404, https://doi.org/10.5194/angeo-36-381-2018, 2018.

Van Geffen, J., Van Weele, M., Allaart, M., and Van der A, R.: Royal Netherlands Meteorological Institute (KNMI), TEMIS UV index and UV dose operational data products Dataset, 2017, version 2, [data set], available at: http://www.temis.nl/uvradiation/UVindex.html, last access: 1 June 2021.

WHO: Report of the WMO Meeting of Experts on UV-B Measurements, Data Quality and Standardization of UV Indices, Les Diablerets, 25–28 July 1994, 1995.

WMO: Scientific assessment of ozone depletion: 2018, Global Ozone Research and Monitoring Project-Report No. 58, 588 pp., 2018.

Wright, C. Y., Brogniez, C., Ncongwane, K. P., Sivakumar, V., Coetzee, G., Metzger, J.-M., Auriol, F., Deroo, C., and Sauvage, B.: Sunburn Risk Among Children and Outdoor Workers in South Africa and Reunion Island Coastal Sites, Photochem. Photobiol., 89, 1226–1233, https://doi.org/10.1111/php.12123, 2013.

Zempila, M.-M., van Geffen, J. H. G. M., Taylor, M., Fountoulakis, I., Koukouli, M.-E., van Weele, M., van der A, R. J., Bais, A., Meleti, C., and Balis, D.: TEMIS UV product validation using NILU-UV ground-based measurements in Thessaloniki, Greece, Atmos. Chem. Phys., 17, 7157–7174, https://doi.org/10.5194/acp-17-7157-2017, 2017.